A. W. Ruff

NBSIR 76-992

Studies of Deformation at Sliding Wear Tracks in Iron

A. W. Ruff

Institute for Materials Research
National Bureau of Standards
Washington, D. C. 20234

February 1976

Final

NAONR-35-75

Prepared for
Office of Naval Research
Department of the Navy
Arlington, Va. 22217

NBSIR 76-992

STUDIES OF DEFORMATION AT SLIDING WEAR TRACKS IN IRON

A. W. Ruff

Institute for Materials Research
National Bureau of Standards
Washington, D. C. 20234

February 1976

Final

NAONR-35-75

Prepared for
Office of Naval Research
Department of the Navy
Arlington, Va. 22217

U.S. DEPARTMENT OF COMMERCE, Elliot L. Richardson, *Secretary*
James A. Baker, III, *Under Secretary*
Dr. Betsy Ancker-Johnson, *Assistant Secretary for Science and Technology*

NATIONAL BUREAU OF STANDARDS, Ernest Ambler, *Acting Director*

Abstract

Determinations of strains have been made on the surface and subsurface on specimens of high purity iron after different amounts of sliding wear have taken place. The method involved the measurement of loss of intensity (contrast) of particular electron channeling lines obtained from small selected areas near the wear track. Through the use of a calibration specimen deformed plastically to a range of strain values, the channeling line contrast loss was related to plastic strain. Strain maps lateral to the wear track and below the original surface were obtained for different total sliding distances by removing controlled thicknesses of iron using electropolishing. In all cases the maximum strain was found at the track center location at the surface and the strains decreased steadily with depth below the track. At 50 g load the strains vanished at about 40 μm depth. Significant strains were found to exist outside the wear track boundaries. The results are compared with other studies previously reported. There was no indication of a soft or less hardened surface layer in any of the specimens studied.

Introduction

An increasing amount of attention has been directed recently toward the analysis of wear debris produced in wearing systems. The opportunity of monitoring the condition of the mechanical system is available through access to the lubricating systems and the debris contained there. However, it is necessary that relations be drawn between the type of debris recovered and the processes under way at the solid surfaces. It is recognized that debris particle sizes and shapes may vary considerably depending on the nature of the wear processes and on the environment experienced by the surfaces. In considering the various aspects of this overall problem that need to be examined quantitatively, one important consideration appears to involve the stress distribution and plastic deformation history associated with the material at the wear track. It is known that these quantities vary from metal to metal and that the microstructure of the material near the surface can have a significant effect on the wear. This present study was concerned with the application of the selected area electron channeling method to the measurement of plastic strains adjacent to and beneath sliding wear tracks produced on iron surfaces. Some microhardness determinations that were made adjacent to the wear tracks for comparative purposes will also be discussed.

Consideration has been given in the literature to various aspects of the stress and plastic deformation present in bodies that are in contact and are wearing. The treatments principally involved asperity interactions[1,2] and indentation loading[3] rather than a complete elastic-plastic analysis around the wearing contact. Experiments

involving the variation of wear track width with load and deformation patterns beneath a wear track have been reported.[4] Studies in sliding[5] and rolling[6] contact have concentrated on the developing strains and the wear track width in steel, aluminum and copper. Recently, Suh and coworkers[7,8] have examined theoretically and experimentally the consequences of plastic deformation associated with sliding wear. Their theory (the "delamination" theory) is concerned with the microstructural pattern that develops around a wear track, and to some extent, explains quantitative differences between the responses of different metals to wear. Two significant features of their model are (i) a "soft" or low dislocation density region near the surface of the wearing solid and (ii) void and/or crack formation at characteristic distances below the wearing surface. Some of the information derived from the present study of subsurface strains is pertinent in connection with that theory.

Experimental Method

A constant velocity, sliding wear tester was constructed for use in these studies. The instrument is shown in Fig. 1. A motor driven cam transmitted a reciprocating velocity of 2.0 cm/s to a platform on which a small tray was fastened containing the test specimen. The linear motion was adjustable up to 2 cm in length. A loading pin was in contact with the specimen from above with a load determined by a dead-weight loading system. A bearing ball was clamped at the end of this pin in contact with the specimen. The loading pin was fastened to an elastic beam containing two mounted strain gauges. The frictional force at the contact surface could be measured during the wear

test using this strain gauge signal. Tests of durations from 5 to 1000 cycles (up to 40 minutes) were conducted under either dry or oil lubricated conditions.

The oil and wear debris could be recovered after a test by washing the specimen and tray with a solvent. Filtration through a micrometer pore sized filter (typical hole size 1 μm) enabled recovery of the debris for later examination. Careful washing and cleaning (without mechanical action) usually also left some debris on the specimen surface near the wear track.

Specimens were fabricated from electron beam melted iron sheet, 0.5 mm thick with a total impurity content of 150 ppm (principally 10 ppm C, 110 ppm O, 12 ppm N). Specimens were cut to size 1 cm x 2.5 cm and then annealed for 2 hours at 900°C in a small, evacuated, sealed quartz tube. Prior to wear testing each sheet specimen was electropolished between 10 and 15 minutes in a solution of 6% perchloric acid and 94% glacial acetic acid. In experiments involving strain measurements below the worn surface, the same electropolishing procedure was followed in order to remove material in a strain-free manner. Under the conditions used, an approximate depth of 25 μm of iron was removed from each side of the sheet in 14 minutes. Specimens were clamped down around the edges within the specimen tray in the wear tester. Particular care was taken not to mechanically damage the specimens during installation (except for the edge regions as noted above).

The loading pin consisted of a 2.4 mm diameter type 52100 steel ball affixed to the end of a rod on which the load was applied so that it could not rotate. Balls were used for one or more tests depending

on the amount of wear accumulated. In those tests involving oil lubrication, the specimen tray was filled with SAE 30 weight automotive oil prior to testing. The oil had been previously filtered through a 1.2 μm filter to remove solid impurities.

Wear tests were conducted by mounting the electropolished specimen in the tray, adding oil if desired, loading the pin to the desired value, starting the drive motor and carefully lowering the pin into contact with the specimen. The initial few cycles of signal recorded from the strain gauges monitoring the friction force were usually not reliable but very shortly the friction coefficient could be reproducibly determined.

The wear specimen and bearing ball were examined after each test and after cleaning with a solvent using optical microscopy and scanning electron microscopy (SEM) techniques. The SEM available had been modified for selected area electron channeling pattern (SACP) studies involving the rocking beam mode[9,10] of operation. The specimen was always oriented normal to the electron beam and operated in the emissive (secondary and backscattered electron) mode. The minimum selected area realizable was about 10 μm across (approximately circular) at a specimen-lens distance of 2 mm. The angular extent of the SACP was about 15 degrees under those conditions. The microscope was operated at 20 kV and a specimen current of 2×10^{-7} amperes. A discussion of the SACP method is given in the appendix.

Results and Discussion

A. Selected Area Channeling Patterns

Previous workers[9-11] have used either the line width or the contrast associated with a particular channeling line as a measure of the strains present in the channeling volume. It is known that channeling lines of different hkl indices (corresponding to the hkl of the planes involved in the channeling process) exhibit different broadening amounts even though the different lines originate from the same volume of deformed crystal. The higher index lines are more sensitive to lattice strain. Hence it is necessary to systematically employ the same type of channeling line and to calibrate the effect of strain on the line using a suitably deformed specimen. In this study the 220 (in a few cases the 200) channeling line in iron was measured. The contrast of the line was determined according to the relation $C = [I(max) - I(min)]/I(avg)$ where I is the detected (amplified) signal level. Proper use of the gain and DC level controls on the SEM permitted the contrast values to be determined quantitatively from photographs of the signal trace on the recording screen. An example of an SACP taken from one grain in an iron specimen is shown in Fig. 2a. Superimposed on the pattern is one signal trace and two signal reference levels used in measuring the contrast value. The upper reference corresponds to the maximum signal level (white) and the lower to the minimum signal level (black). The vertical deflection gain control is used to establish the difference between these two levels at a fixed value for all measurements. The DC level control then is used to depress the signal level by an integral multiple of full scale while the signal gain control is increased to maintain the signal between the reference levels. It was possible to obtain reproducible contrast values over the range of

0 to 10% by following this procedure, provided that each specimen was mounted carefully in the SEM in a reproducible manner. Figure 2b shows a set of signal traces from which the average contrast value of 7.2 ± 0.5% was determined in this example. (The DC level is displaced by two full scale units in this example.) It was possible to obtain the average contrast value for a particular region in a specimen in a period of about 5 to 10 minutes using this method. Repeated measurements indicated that a reproducibility of about 10% in any determined contrast value could be obtained.

B. Polycrystalline Iron Calibration Specimen

A rod, 3 mm in diameter, of electron beam melted iron was cut to a length 20.3 mm. Two flat surfaces were ground on opposite sides of the cylinder, one parallel to the rod axis, the other at an angle of about 7° to the axis. This resulted in a tapered specimen, 1.3 mm thick at one end and 1.7 mm thick at the other end. The specimen was then electropolished, sealed in an evacuated capsule and annealed for 2 hours at 940°C. The specimen was then deformed in compression between two steel plates on which teflon films had been placed until a uniform thickness of 1.3 mm was reached. Examples of the grain and surface structures at two locations along the specimen are shown in Fig. 3. SACP from two different regions of the specimen are presented in Fig. 4. It was not difficult to locate a sufficient number of grains with 220 channeling bands prominent in their patterns in order to map out the contrast gradient that resulted from the introduced strain gradient along the bar length. The calculated strain gradient is shown in Fig. 5. Davidson[12] has previously employed a calibration specimen deformed in

tension in a study of deformation using SACP methods without, however, conducting quantitative signal contrast measurements.

Measurements were conducted to determine the variability in contrast within one channeling band from a given region in the specimen. In one case 13 measurements were made at different locations along a 220 band resulting in an average contrast value of $\overline{C} = 7.2 \pm 1.1\%$. Another region in a different grain resulted in a contrast value $\overline{C} = 6.2 \pm 1.0\%$ for 14 measurements. [In these cases locations along the contrast band where fine structures were present and produced anomalous variations in line contrast were intentionally avoided. These fine structures, some of which can be seen in Fig. 2a are, in fact, high index channeling lines.] In some grains both 200 band and 220 band measurements could be made and compared. Some results given in Table I showed that the difference in average contrast value between these two bands was usually small and within the scatter found for one band. While this result would clearly not be true for all channeling bands, it indicates that selected band comparisons can be made. In this study only contrast values of 220 bands were used in the strain analysis study. The results of SACP contrast measurements in grains along the length of the calibration specimen are given in Fig. 5. Contrast values below 1% were not measured due to poor precision. These data seem reasonably well described by a linear decrease of contrast along the length of the specimen in the direction of increasing strain. The resulting strain vs. SACP contrast relation is shown in Fig. 6. Strains greater than about 17% cannot reliably be determined by this method. Previous studies of stainless steel[9,10]

have shown that strains in excess of about 20% (tensile) could not be reliably measured using SACP methods.

It should be emphasized that while the linear relation shown in Fig. 6 between the SACP contrast and strain does adequately fit the experimental data, it is without theoretical justification. In fact the SACP can be recognized at strains greater than 20% but precise measurements are difficult. Schulson[13] has presented a simple analysis of the effect of strain on SACP lines that describes the strain in terms of rotations of the lattice planes involved in channeling. This analysis is summarized in the Appendix. Using this approach a calculated shear strain vs. SACP contrast curve was obtained and is shown in Fig. 6. The curve is normalized at C = 8.5% with the experimental data. The agreement with the experimental data is not good particularly for strains around 10%, however, many of the assumptions involved in the analysis are not closely fulfilled in the experimental situation. One gains from these considerations some idea of the potential accuracy of the SACP method for strain determination.

C. Sliding Wear Experiments

A series of wear experiments were conducted using progressively larger total sliding distances. The load in all experiments reported here was 50 g and the sliding speed was 2.0 cm/sec. The specimen surfaces were all electropolished for about 10 minutes immediately before wear testing. The oil lubricated tests will be described first.

The least sliding distance attempted was 0.17 m involving 5 machine cycles. The nature of the contact varied greatly along the track and in many cases the track appeared interrupted by regions of noncontact

with the loading ball. The electropolished surface did typically contain an undulating texture so that the degree of contact could be expected to vary. A number of areas in and adjacent to the wear track were selected and SACP obtained. The strains determined from these using the contrast-strain relation (Fig. 6) are shown in Fig. 15 and will be discussed later. Patterns were taken from areas of apparent noncontact and showed that no additional strains were present in those areas compared to undisturbed surface regions.

The sliding distance was then increased to 1.7m under the same conditions in other respects. The typical wear track was continuous (Fig. 7) but with small regions where the original surface could be seen within the track. The grain structure of the specimen can be seen in Fig. 7 as a result of channeling-type of contrast due to an orientation-dependent emissive signal contribution. The marked locations are those from which the SACP were taken; two of these (A and E) are shown in Fig. 8. The loss of contrast in the 220 band (arrow) comparing position A remote from the track with position E at the wear track center is apparent. The strain values determined are discussed later.

Tests conducted at a sliding distance of 17 m showed that in all cases the wear track was continuous and well defined except at the edges. In certain regions where deep pits existed in the initial surface, those features could still be recognized. Figure 9 shows a portion of such a track (taken at high contrast to emphasize the grain and track structure) with some interesting detail at the edges. When the accumulated deformation is still low, apparently the channeling contrast difference between neighboring grains can be sufficient to permit

identification of the grain boundary beneath the edge of the wear track, that is beneath a thin layer of deformed material (see arrow, Fig. 9). Figure 10 shows some detail near an initial pit in the track. Evidence of rubbing in the sliding direction can be seen on the bottom of this depression, probably due to debris particles momentarily trapped within the depression and supporting some of the load. The fine, pebbled appearance of the surface at the right of the depression (Fig. 10b) was frequently observed and may be indicative of the oxide film at the surface. SACP signal traces obtained from the center and the edge of this wear track at a depth of 10 μm below the original surface are shown in Figs. 11a and 11b, respectively. The loss of contrast at the 220 band (arrow) within the wear track can be seen.

A representative portion of the wear track generated at a sliding distance of 170 m is shown in Fig. 12. Under these conditions the track edges are well defined and none of the original surface structure remains to be seen in the track. Ridges of material oriented parallel to the sliding direction are a principle feature of the wear track appearance. This specimen was examined in the SEM before careful cleaning and many debris particles remained on the surface. A more detailed view of the end of the track is shown in Fig. 13. Many debris particles remain in this area. Two of the larger particles are shown in Fig. 13b (arrows). They appear flat and laminar in shape and are about 7 μm in lateral dimensions. In the region to the left, there is evidence for extensive plastic flow of the near-surface material in the wear track region, a common observation in this study. It appears

that the flat laminar particles are produced by extensive plastic flow of the wear track surface material until a fragment eventually breaks loose.

The appearance of wear tracks formed under dry conditions was similar to the appearance of tracks obtained in oil lubricated tests. Figure 14 shows a portion of the track in one dry sliding test of sliding distance 17 m. The appearance can be compared with the track in Fig. 9. Somewhat greater height associated with the ridge features in the track is seen under dry conditions. SACP traces from the track edge and at a location distant from the track edge are shown in Figs. 14b and 14c, respectively. The 220 channeling band is marked.

Wear coefficient and wear volume values were determined in two of the oil lubricated experiments through measurements on the ball used in applying the load to the specimen. At 50 g load and 17 m distance, the wear volume was $\Omega = 0.8 \times 10^{-8} cm^3$ and the wear coefficient was $k = 3\Omega \cdot H/L \cdot D = 1.5 \times 10^{-5}$ where H, L, and D are hardness, load, and sliding distance, respectively. At 100 g load and 240 m distance, $\Omega = 4.3 \times 10^{-8} cm^3$ and $k = 2.7 \times 10^{-5}$. Under dry conditions both values were considerably greater.

D. Strain Measurements at Wear Tracks

Shortly after each wear test was completed, SACP were obtained from the original surface at positions of various distances from the wear track center. A grain was selected that was sufficiently large and located across the track from which all the SACP were obtained. At each location at least four values of contrast across the 220 band were obtained and averaged. The associated strain value was determined from

the calibration curve (Fig. 6). The results are given in Fig. 15. A common feature of the lateral strain distribution is the rapid decrease in strain near and beyond the edge of the wear track. However, the surface strains still extend condsiderable distances from the apparent edges of the wear tracks (arrows in Fig. 15). For example, at a sliding distance of 17 m under oil, the strain at the track edge (45 μm) was about 11% and decreased to about 3% at twice that distance from the center (90 μm). In two cases the strain could be measured over the entire track width and was found to increase steadily as the track center was approached. Since strains greater than about 18% could not be measured by this method it was not possible to map out the entire surface distribution of strains in all cases. However, it appears that for sliding distances up to 17 m (and possibly beyond) the maximum strain values at the surface are found at the track center location. Comparison of the 17 m sliding distance experiments under dry and oil lubricated conditions reveals that larger strains and a broader distribution are produced under dry conditions but otherwise the strain distribution is similar.

Measurements of the strain distribution with depth below the original surface were conducted after electropolishing for appropriate times to remove a specific thickness of material. The original track center was located with reference to adjacent grain boundary junction locations. Some uncertainty in position probably arose due to the change in grain boundary locations with depth through the specimen. However, the use of two or three such reference locations in each case probably kept that uncertainty to about ±10 μm. The results of two 17 m sliding distance experiments are shown in Fig. 16. In both cases the

measured strains extend further lateral to the wear track than its edges (marked by arrow) even at subsurface locations. Near the track center the maximum strains are found at the surface and decrease smoothly with depth, vanishing at 30 μm and 40 μm under oil-lubricated and dry conditions, respectively. However, outside of the track edge location it appears that the maximum strains are located subsurface, about 10 μm deep in these experiments. At any specific depth, however, the maximum strain was found under the wear track center.

Recently Popov and Titukh[14] have used X-ray diffraction methods to study the stresses in several steels at various depths below the surface of specimens that had been tested for abrasive wear resistance. Measurements of diffraction line broadening were converted to dislocation density values in the usual manner. Their results on one steel (type 270 Kh 12 BI: 2.7% C, 1.2% Cr, 0.35% Ni, 0.35% Mn, 0.4% Si, 0.3% P, 0.3% S) are shown for the austenite phase in Fig. 17a. The dislocation density (ρ_D) decreases rapidly with depth from the original surface and is reduced by one order of magnitude at a depth of 15 μm. The other alloys studied showed essentially the same behavior; those with larger values of dislocation density at the surface also retained larger values to greater depths in the material. In all cases the largest values of ρ_D were found at the specimen surface. Using the usual relation that strain $\propto \rho_D^{1/2}$ and Kehs[15] data on iron relating ρ_D and elongation, equivalent strain values are plotted in Fig. 17b. These X-ray derived results are clearly consistent with the SACP derived results of the present study. It is probably not valid to compare independently obtained data using these two methods even on the same material unless

some consistent method of strain calibration is utilized. It is worth noting that the X-ray measurements involve lattice planes nearly parallel to the specimen surface in contrast to the SACP method which utilizes lattice planes nearly perpendicular to the specimen surface.

While no results on the strains developed beneath sliding wear tracks were provided, Ronay[16] has reported an increase in the track width with increasing number of cycles as observed in this study. Ronay further reported on apparent work-softening associated with reciprocal rather than unidirectional sliding, an observation that indicates the possible sensitivity of the developing deformation structure on the details of the wear and loading geometries.

Dautzenberg and Zaat[17] have reported on quantitative determinations of deformation associated with sliding wear using a geometric method that measures the change of grain shape with deformation in the material. The deformation there represented accumulated plastic strain in the specimens. They reported a smooth decrease of effective deformation with increasing depth below the wear track in copper, down to a depth of about 100 μm. Note that the strains measured in the present work in iron by the SACP method also represent total (compressive) plastic strain through the use of a calibration specimen. It would be of interest to compare the two methods quantitatively.

E. Microhardness Measurements Beneath the Wear Track in Cross Section

Many studies have been conducted using indentation microhardness methods for the purpose of determining the level of deformation locally in materials after wear (and other mechanical) tests. The advantage of the microhardness method is its simplicity and speed,

however, the interpretation of the results in terms of stress level or other microstructural variables is not well understood. Nevertheless relations between flow stress and indentation hardness, for example, have been described.[18] A wear specimen (17 m sliding distance) was cross-sectioned, metallographically prepared and electropolished lightly to remove preparation damage. Microhardness determinations were then made using a Knoop indenter and a 10 g load at various distances from the original surface both under the wear track center and remote from the wear track. The long axis of the indenter was aligned parallel to the surface trace. The results of these measurements are shown in Fig. 18. The hardness values for the undisturbed specimen region were nearly constant at a value of 100. However, at a distance of 5 μm from the original surface the hardness abruptly decreased by nearly 50%. This decrease was clearly due to flow of material away from the indentation site as a result of the loss of constraint as the free surface is approached. That is, accurate microhardness values could not be determined within about 10 μm of the free surface due to relaxation effects at that surface. Indentations under the wear track center at different distances from the original surface showed that the hardness increased as the surface was approached. Measurements closer than about 20 μm to the original surface were not attempted due to the demonstrated relaxation effects experienced there. The microhardness variation with depth below the wear track was in reasonable agreement with the strain variation found here (Fig. 17) except that the hardness method is not believed suitable for regions close to the free surface.

Microhardness measurements in aluminum after sliding wear testing have been reported by Savitskii.[19] His results for undeformed aluminum

show a small decrease with distance from the surface (on cross-sectioned specimens) but measurements were not made any closer than 20 μm to the surface. However, on specimens that had been tested in sliding wear, he reported measurements as close as 5 μm to the free surface. The result in each case was a decrease in microhardness value near the surface and also at some distance away, that is, a peak in microhardness was found at depths of 10 to 15 μm. While that peaking tendency has been cited[20] as evidence for a softening of the near surface region of the wear track, it was not established that the microhardness measurements were unaffected by proximity to the free surface.

Tsuya[21] has reported microhardness values for copper tested in sliding wear. He noted that the hardness rapidly decreased with depth below the surface on cross sections at the wear track center. In contrast to that, Kirk and Swanson[22] have recently reported a zone of low microhardness very near the wear surface in copper also tested in sliding wear. The latter work did not report hardness measurements near an unworn surface so that the relaxing effect expected near the surface cannot be eliminated from their data.

There is some disparity in the reported trend of microhardness results with distance from a wear track surface and further careful studies are indicated. However, it is well to keep in mind that such measurements are complicated measures of the average resistance to indentation deformation in the material. Anisotropic effects in such measurements also have been reported.[21]

F. Relation of Present Results to the Delamination Theory

One of the purposes of the present study was to improve the understanding of the strain patterns that develop beneath a sliding wear track as a function of several important parameters. In order to study the initial stages in the development, relatively low loads and a progression of sliding distances were studied. There was no indication of severe wear or large wear debris particles in any of the oil lubricated tests; the dry tests did show an increased wear coefficient into the mild wear regime. Suh et al.[20] have reported dry wear test results on iron, iron with small amounts of tungsten added, and several types of steel (1010, 1018, 1020). Subsurface delamination was reported for many of these tests, at however a higher wear coefficient than found in the present study (approximately $k = 0.4$ to 3×10^{-4} compared to $k \simeq 2 \times 10^{-5}$ here). Thus we can regard the present study as indicative of the early stages of wear and deformation. It is planned to continue this study to the heavy wear regime.

One unique feature of the delamination theory is the existence of a soft or low-dislocation density region near the wearing surface. Suh et al.[20] have evaluated the thickness h of that region assuming film-free conditions at the surface. For copper they calculate $h \simeq 10\mu m$ and for Fe-3% Si, $h \simeq 0.1$ μm. Applying that same procedure to iron where the flow stress $\sigma = 20$ MPa, the shear modulus $G = 84$ GPa, the Burgers vector $b = 2.5 \times 10^{-8}$ cm, and Poissons ratio $\nu = 0.28$ the thickness of the low dislocation density zone is calculated to be $h \simeq 0.12$ μm. Thus the effect of image forces on reducing the stress level and dislocation density in iron should be observable in the first 1000 Å, approximately. The SACP obtained in this study are derived from electrons

generated in the near surface layer, probably within 500 Å of the surface. (Note that backscattered primary electrons that penetrate to these depths will contribute to secondary electron emission from within 50 Å of the surface upon exiting.) Thus the SACP obtained from the as-worn surface in iron are associated with the near-surface layer that is of interest in the delamination theory. Apparently this layer shows a maximum strain in the present experiments on iron rather than any softening or lower hardness behavior. Consideration of the image formation process in SACP generation would suggest that softening in the nearest 100 Å to the surface might not be detectible but that the uppermost 1000 Å is precisely the region from which the preponderant signal originates.

Summary

(1) The selected area channeling pattern method can be utilized to measure strains associated with wear deformation both at the original surface and subsurface after electrochemically removing material.

(2) Strains up to nearly 20% can be measured in iron by this technique. The use of proper signal averaging techniques along one particular channeling band can lead to reproducible contrast measurements.

(3) The maximum strains associated with the wear track, under low wear conditions and probably involving the early stages of wear deformation, are always found at the surface and the track center. At locations outside the track edge, the largest remaining strains appear to be located below the original surface.

(4) The soft or low dislocation density zone postulated by the delamination theory (for film-free surfaces) was not found in these experiments on iron. Calculation indicates that zone should be 1000 Å deep, approximately, and detectible using this method.

Acknowledgments

Many fruitful technical discussions were held during the course of this research with various colleagues, including Richard Miller, Nam Suh, Vernon Westcott, Lewis Ives, and others at NBS, and their contributions are gratefully acknowledged.

Appendix A. Indentation Deformation

It was of interest to apply the SACP strain measurement method to another mode of deformation than wear in order to further explore the technique. An indentation experiment was conducted using a spherical indenter of radius 0.80 mm and a vertical load of 3kg. The specimen was prepared in the same manner as the wear test specimens prior to indentation. The specimen was backed by a hard steel plate during loading, however, clear evidence of the indention location could subsequently be seen on the back surface of the specimen indicating that the specimen thickness (approximately 0.4 mm) was insufficient for any bulk material approximation. Figure A1 shows the surface after indenting and indicates the locations, A through F, at which SACP were obtained at the surface. Three subsurface sections were subsequently obtained by electropolishing. These were at depths of 35, 70, 120 μm below the original surface. SACP were obtained at these levels and the strain values determined using the calibration curve (Fig. 6). The location of the indentation center could be visually located at each level and further position reference was possible using two triple grain junctions nearby. The lateral position uncertainty below the original surface is believed to be not more than ±20 μm. Figure A2 contains four SACP taken from the indicated locations at a depth of 70 μm from the original surface. The 220 channeling band is vertical and its loss of contrast as the indentation location is approached can be seen. The appearance of the specimen after electropolishing to the final level (120 μm deep) is seen in Fig. A3. The grain around the indentation center (marked Δ) from which all SACP were taken can be seen.

The strain configuration determined in a vertical plane through the indentation is shown in Fig. A4. A vertical-to-horizontal expansion of two was used in constructing this figure. The strain values circled are in percentage and are placed at the locations where they were determined. The indentation is shaded. Approximate strain contour lines have been sketched in the figure. There is some degree of symmetry to the strain pattern measured in that strains of about 15% are found 100 μm distant from the indentation center both vertically below and lateral to it. At a distance of 300 to 400 μm the strain values are essentially that of the undeformed specimen. A tendency for an increase in subsurface strain values is seen at some distance from the indentation. Underneath the indentation, the strains decrease smoothly with depth. This same type of distribution was found around the wear tracks discussed earlier.

The elastic solution to the indentation problem would predict a maximum pressure of about 1000 MPa. The corresponding maximum shear stress would be 300 MPa at a depth of 50 μm, considerably in excess of the flow stress of this material of about 20 MPa. According to Shaw and DeSalvo[23] the boundary of plastic behavior beneath the indenter would extend at least about 220 μm deep. This is consistent with the data in Fig. A4 that shows strains of 15% at a depth of 120 μm and strains of 5% at a lateral distance of 220 μm.

Appendix B. Selected Area Electron Channeling Method

The technique for obtaining electron channeling patterns from small areas of a crystalline specimen using the "rocking beam" approach has been described previously.[9,10] Briefly, the excitation currents through the final two lenses and the drive currents applied to the scanning coils are controlled so that the beam focus on the specimen surface is as nearly stationary (in position) as possible in the SACP mode. The scan current causes the beam to sweep angularly about the electron optical column axis. The angular range is adjustable from about 18° down to smaller values. In the image mode (obtained by altering the scan coil-current configuration) the beam sweeps in position describing a rectangular raster on the specimen surface. It is possible to switch simply from one mode to the other during examination of the specimen. Figure B1a shows an image of an electropolished surface of iron taken in the image mode at a magnification of about 150X (magnifications up to 2000X can be used conveniently). Switching the operation to the SACP mode produced the pattern shown in Fig. B1b, obtained from a region in the center of the above area of lateral dimensions about 10 μm. The pattern in this example is slightly enlarged to reveal the fine detail associated with the different channeling lines. The information contained within the SACP can be considered an average over the microvolume irradiated by the beam, although in fact the beam position does trace a regular but complicated path throughout that volume during one scan frame. For this and other reasons it is best to obtain several contrast measurements from a channeling band of interest in one frame and then average those determinations. This procedure also minimizes the effects of high index bands that intrude on the band of interest.

Schulson[13] has presented a simplified analysis of channeling line broadening that seems to agree well with some observations in the present study. He considers the distorted regions of the microvolume involved in the channeling process to be described by local rotations ϕ of the channeling planes (similar to some treatments of X-ray diffraction from deformed material). Using a two-beam approximation (incident and diffracted beam), the deviation parameter $\tilde{s}$ which measures the deviation from exact Bragg conditions is changed an amount

$$|d\tilde{s}| \simeq \phi \cdot |\tilde{g}|$$

where $\tilde{g}$ is the diffraction vector and other effects due to the deformation are neglected in comparison. The dynamical theory calculation of the lattice distortion effect is done for various values of ϕ and $\tilde{g}$ and the results are graphically displayed in reference 13. In order to relate the calculated contrast curves to strain in the present study it was assumed that the angular rotations ϕ were proportional to the local shear strain value ε. The calculated contrast-strain curve was fitted to the measured contrast value for $\varepsilon = 0$. The result is shown in Fig. 6 and was discussed previously.

Other attempts to calculate SACP line contrast (and width) values for undistorted and also for distorted crystals have been reported. Recently Spencer[24] has completed multibeam calculations of SACP profiles in several different materials. He considered the effects of dislocations directly on the channeling process and calculated SACP contrast vs. dislocation density. The agreement with experiments in stainless steel is fair. Additional experiments appear to be needed as well as some improvements in the theory before close comparisons can

be made. The undistorted crystal contrast value of 9% measured[24] for copper 220 bands was significantly higher than the best calculated value of 4%, although a better agreement was found for gold.

Table I. Comparison of average contrast value at channeling bands indicated in different grains in iron.

	200 band		220 band	
Grain	Average Contrast (%)	Std. Dev. (%)	Average Contrast (%)	Std. Dev. (%)
A	2.8	0.3	2.8	0.1
B	1.9	0.2	1.9	0.3
C	3.2	0.9	3.3	0.5
D	2.3	0.3	2.4	0.4

References

1. F. P. Bowden and D. Tabor, Friction, lubrication and wear: A survey of work during the last decade, Brit. J. Appl. Phys. 17 (1966) 1521-1544.

2. E. Rabinowicz, Friction and Wear of Materials, Wiley, New York (1965).

3. M. C. Shaw and G. J. DeSalvo, On the plastic flow beneath a blunt axisymmetric indenter, Trans. ASME, (1970) 480-494.

4. F. B. Bowden and D. Tabor, The friction and lubrication of solids, Oxford (1964).

5. M. Ronay, Dependence of track width on load and on the number of passes in sliding contact, Wear 18 (1971) 187-205.

6. V. M. Radhakrishnan and S. Ramanathan, Plastic deformation in rolling contact, Wear 32 (1975) 211-221.

7. N. P. Suh, The delamination theory of wear, Wear 25 (1973) 111-124.

8. N. P. Suh, S. Jahanmir, E. P. Abrahamson, II, and A. P. L. Turner, Further investigation of the delamination theory of wear, J. Lubr. Tech. 96 (1974) 631-637.

9. R. Stickler, C. W. Hughes and G. R. Booker, Application of the SA-ECD method to deformation studies, SEM/1971 (IITRI, 1971) 473-480.

10. J. P. Spencer, G. R. Booker, D. C. Joy, C. J. Humphreys, Electron channeling patterns from deformed crystals, SEM/1974 (IITRI, 1974) 920-926.

11. D. E. Newbury, The origin, detection and uses of electron channelling contrast, SEM/1974 (IITRI, 1974) 1047-1054.

12. D. L. Davidson, A method for quantifying electron channeling pattern degradation due to material deformation, SEM/1974 (IITRI, 1974) 927-934.

13. E. M. Schulson, SEM electron channeling line width (broadening) and pattern degradation in alkali halide crystals, SEM/1971 (IITRI, 1971) 489-496.

14. V. S. Popov and Yu. I. Titukh, X-ray investigation of transformation in the surface of alloys during abrasive wear, Metal Science and Heat Treatment 17, (1975) 23-26.

15. A. S. Keh, in Direct Observation of Imperfections in Crystals, ed. J. B. Newkirk and J. H. Wernick, Interscience (1962) 213-238.

16. M. Ronay, Dependence of track width on load and on the number of passes in sliding contact, Wear 18 (1971) 187-205.

17. J. H. Dautzenberg and J. H. Zaat, Quantitative determination of deformation by sliding wear, Wear 23 (1973) 9-19.

18. J. J. Gilman, Relationship between impact yield stress and indentation hardness, J. Appl. Phys. 46 (1975) 1435-1436.

19. K. B. Savitskii, cited in V. I. Kragel'skii, Friction and Wear, Butterworth, Washington (1965).

20. N. P. Suh, S. Jahanmir and E. P. Abrahamson, II, The delamination theory of wear, ARPA Progress Report NR 229-011 (1974).

21. Y. Tsuya, The behavior of the layer damaged by friction, Bull. Jap. Soc. Prec. Engg. 2 (1967) 214-221.

22. J. A. Kirk and T. D. Swanson, Subsurface effects during sliding wear, Wear 35 (1975) 63-67.

23. M. C. Shaw and G. J. DeSalvo, The role of elasticity in hardness testing, Metals Engg. Quarterly 12 (1972) 1-7.

24. J. P. Spencer, "Diffraction Contrast in the Scanning Electron Microscope," Ph.D. disertation, Univ. of Oxford (1974).

Figure Captions

Fig. 1 (a) View of sliding wear tester, strain gauge amplifier and chart recorder. (b) Details of constant velocity tester; cam C, push rod P, specimen S, load L, strain gauges G.

Fig. 2 (a) SACP from one grain in iron specimen. The 220 band is prominent; one signal trace is superimposed. (b) A set of signal traces at different locations on SACP showing variation along the 220 band.

Fig. 3 (a) Polycrystalline iron bar specimen, low strain end, after deformation. (b) High strain end showing surface flow and grain structure.

Fig. 4 (a) SACP from grain at low strain (<1%) location in iron bar specimen. Note contrast at 220 band marked B. (b) SACP from another grain at mid-strain (≃13%) location. Note contrast at 220 band marked.

Fig. 5 Calculated strain vs. distance along calibration specimen. Determinations of SACP contrast at indicated positions are shown. Repeated measurements in two grains are also shown (n = 6,14).

Fig. 6 Strain vs. SACP contrast determined from calibration specimen and calculated after Schulson.[13]

Fig. 7 Portion of the wear track after 1.7 m sliding in oil. Locations of SACP obtained are shown.

Fig. 8 SACP at locations (a) A and (b) E in previous figure. Superimposed signal traces show loss of contrast at high strain location.

Fig. 9 Portion of wear track after 17 m sliding test in oil. Note that grain boundaries are detectible beneath edge of track.

Fig. 10 Details at wear track in previous figure. Note deformation marks in pre-existing cavity in track surface.

Fig. 11 SACP traces of 220 band from 17 m sliding test specimen at (a) wear track center and (b) wear track edge locations. at a depth of 10 μm.

Fig. 12 Portion of wear track after 170 m sliding distance in oil. Some wear debris remains on the surface.

Fig. 13 Details at the wear track end in previous specimen. Two large wear debris particles are indicated. Note extensive ridge formation in wear track.

Fig. 14 (a) Wear track portion from 17 m dry sliding test. Traces from SACP obtained at (b) track edge and (c) at one track width distance.

Fig. 15 Strain determinations for various sliding distances and wear track locations.

Fig. 16 Strain determinations at and beneath the original surface for dry and oil-lubricated wear tests.

Fig. 17 Dislocation density and strain comparison between present work and Ref. 14.

Fig. 18 Microhardness measurements on wear test specimen comparing material at and distant from wear track.

Fig. A1 Area of indentation mark on specimen surface and locations from which SACP were obtained.

Fig. A2 Four SACP from indicated positions at a depth of 70 μm below original surface.

Fig. A3 Area of indentation mark at a depth of 120 μm below the original surfce after electropolishing.

Fig. A4 Configuration of strains determined in a vertical plane through the indentation mark. Solid lines are approximate strain contours.

Fig. B1 (a) Electropolished surface of iron single crystal. (b) SACP of specimen, angular range 5 deg., near (113) orientation.

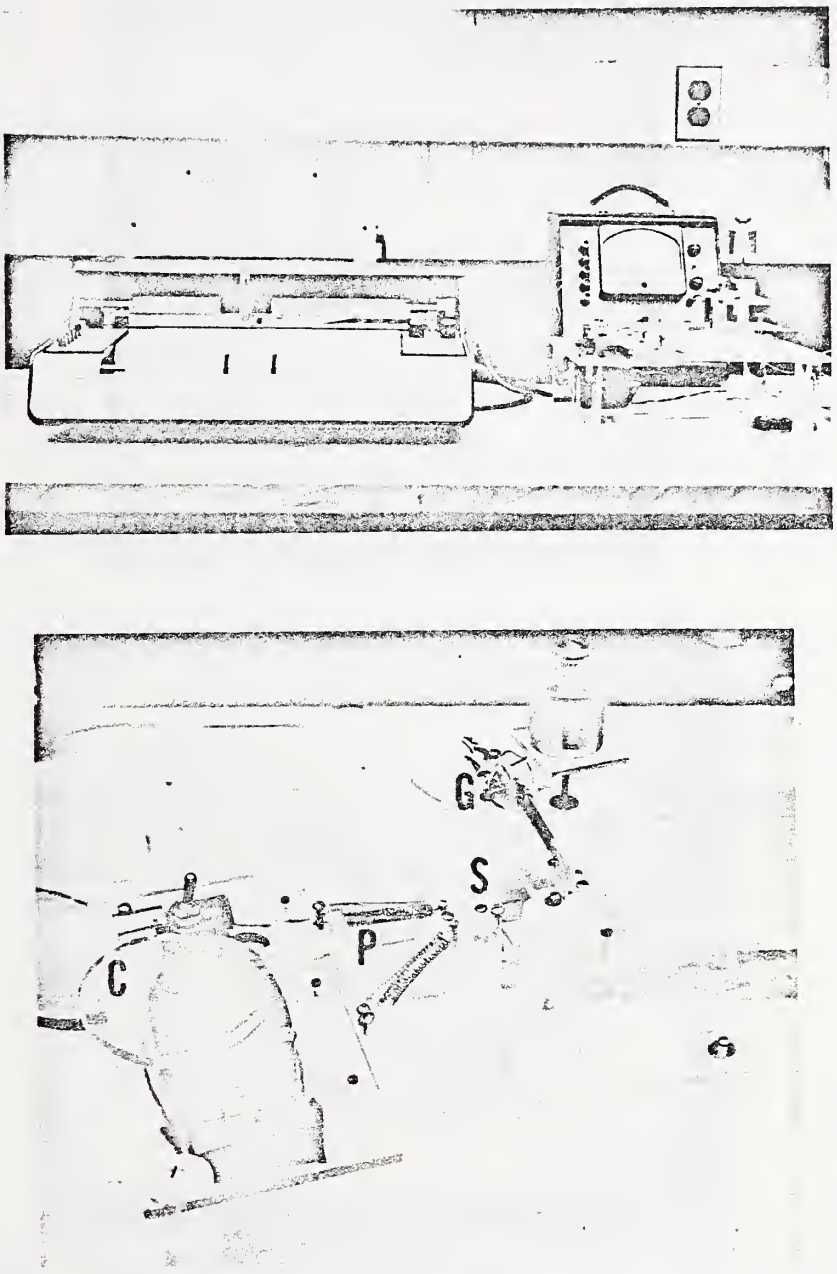

Fig. 1. (a) View of sliding wear tester, strain gauge amplifier and chart recorder. (b) Details of constant velocity tester; cam C, push rod P, specimen S, load L, strain gauges G.

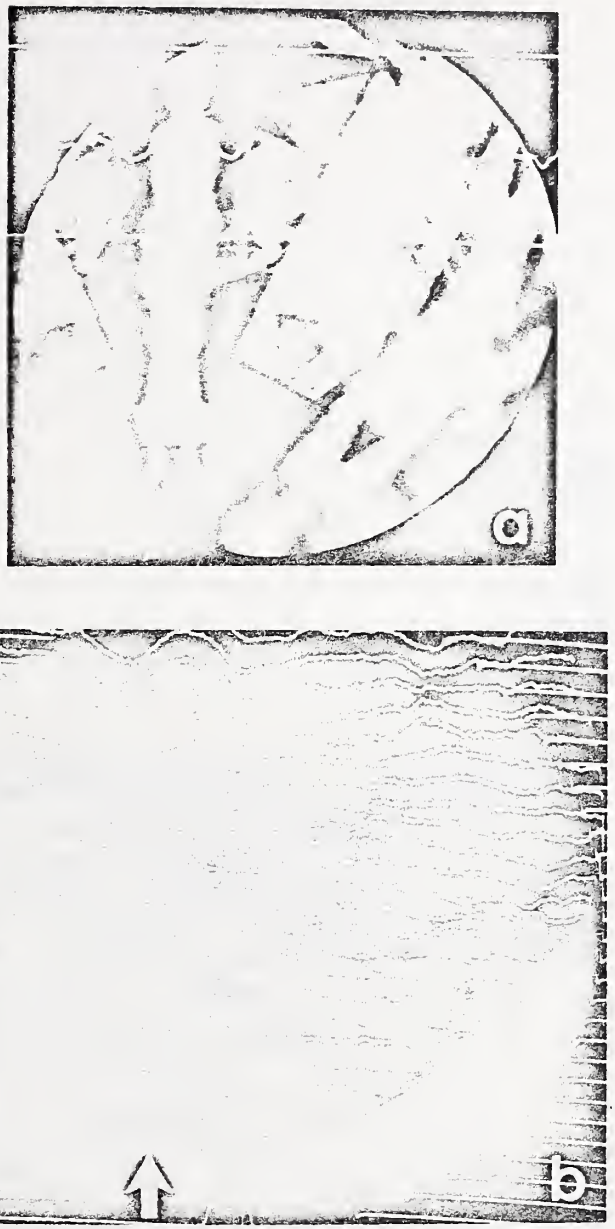

Fig. 2 (a) SACP from one grain in iron specimen. The 220 band is prominent; one signal trace is superimposed. (b) A set of signal traces at different locations on SACP showing variation along the 220 band.

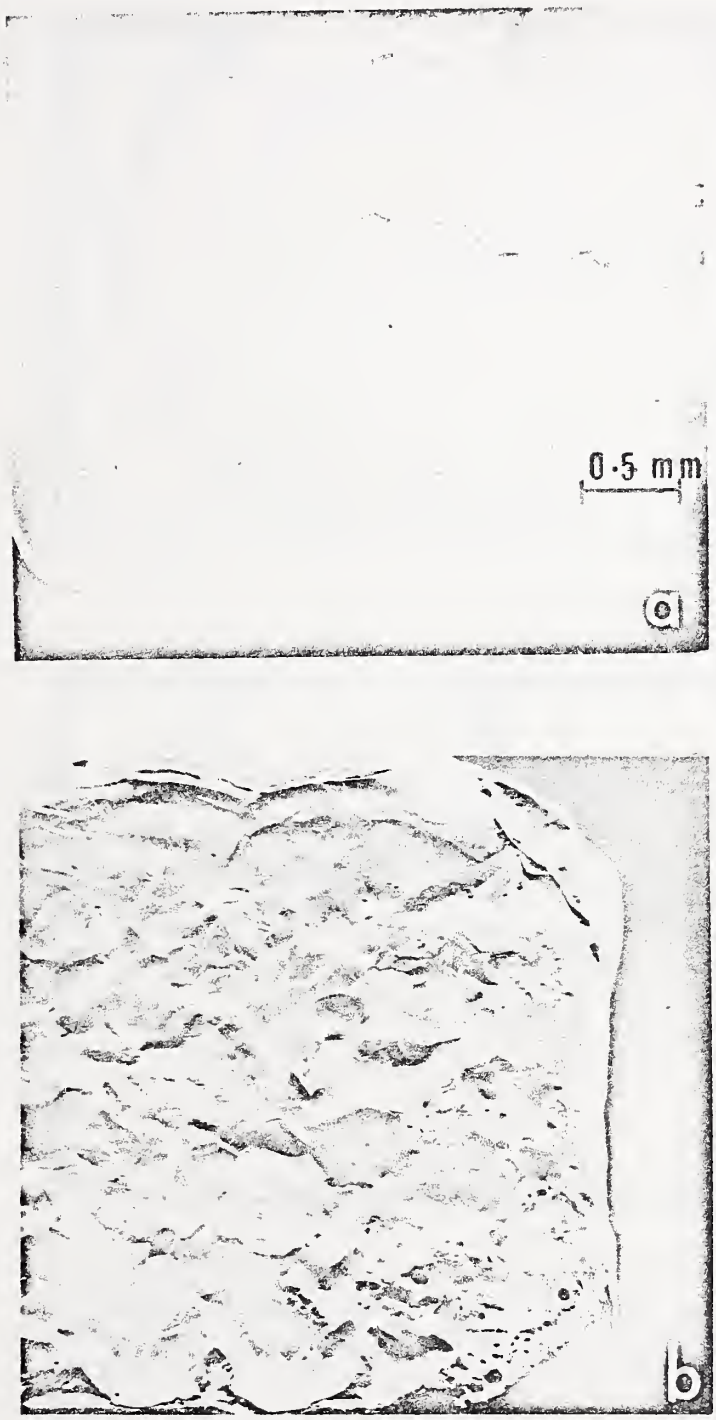

Fig. 3 (a) Polycrystalline iron bar specimen, low strain end, after deformation. (b) High strain end showing surface flow and grain structure.

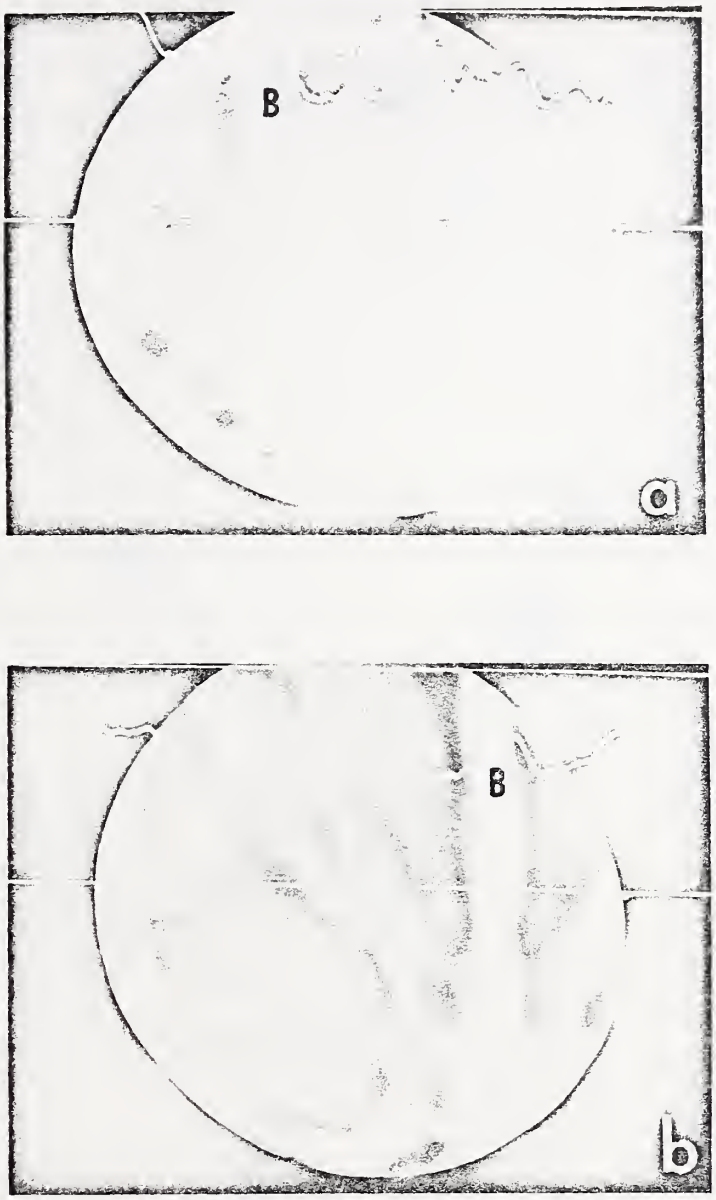

Fig. 4 (a) SACP from grain at low strain (<1%) location in iron bar specimen. Note contrast at 220 band marked B. (b) SACP from another grain at mid-strain (≈13%) location. Note contrast at 220 band marked.

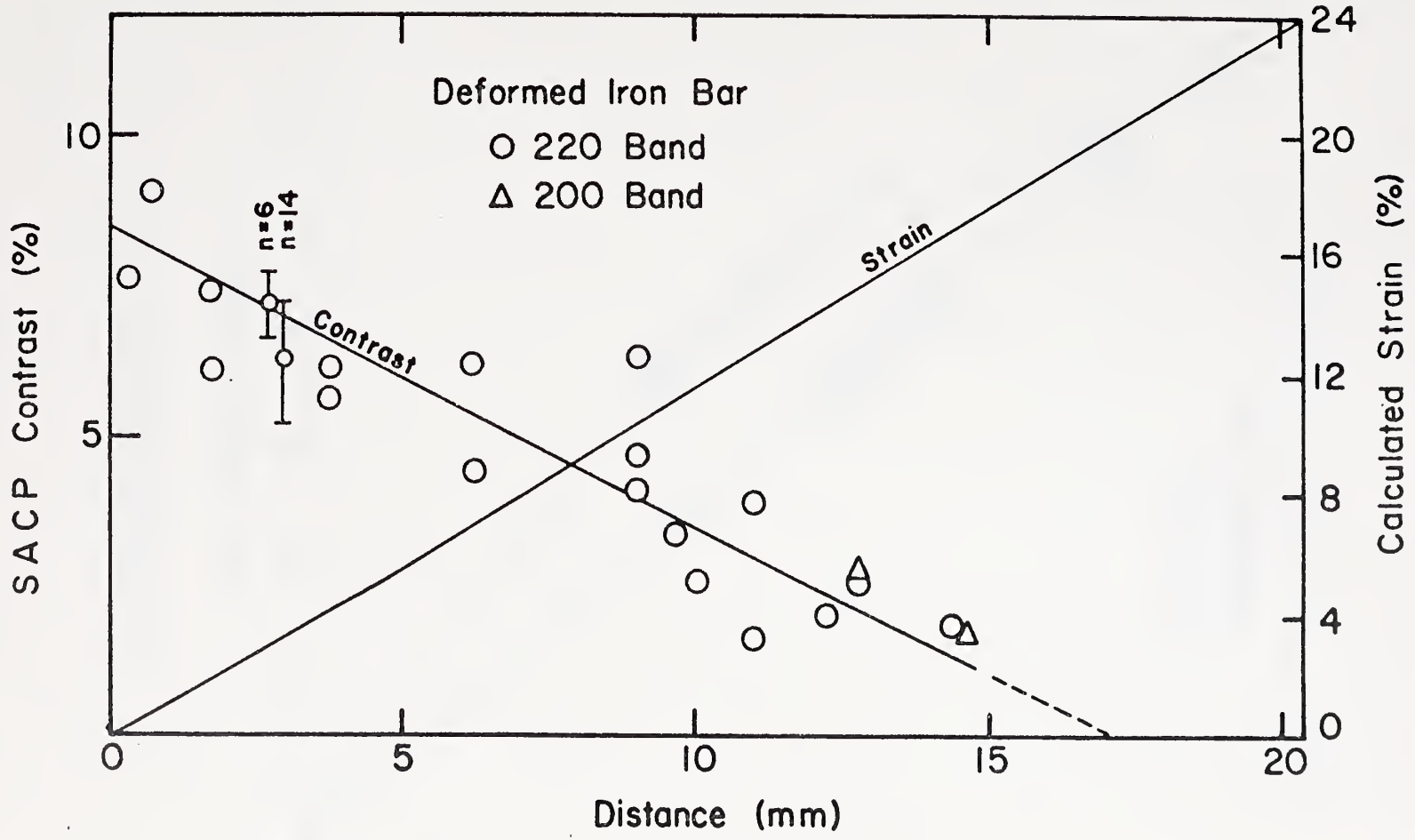

Fig. 5 Calculated strain vs. distance along calibration specimen. Determinations of SACP contrast at indicated positions are shown. Repeated measurements in two grains are also shown (n = 6,14).

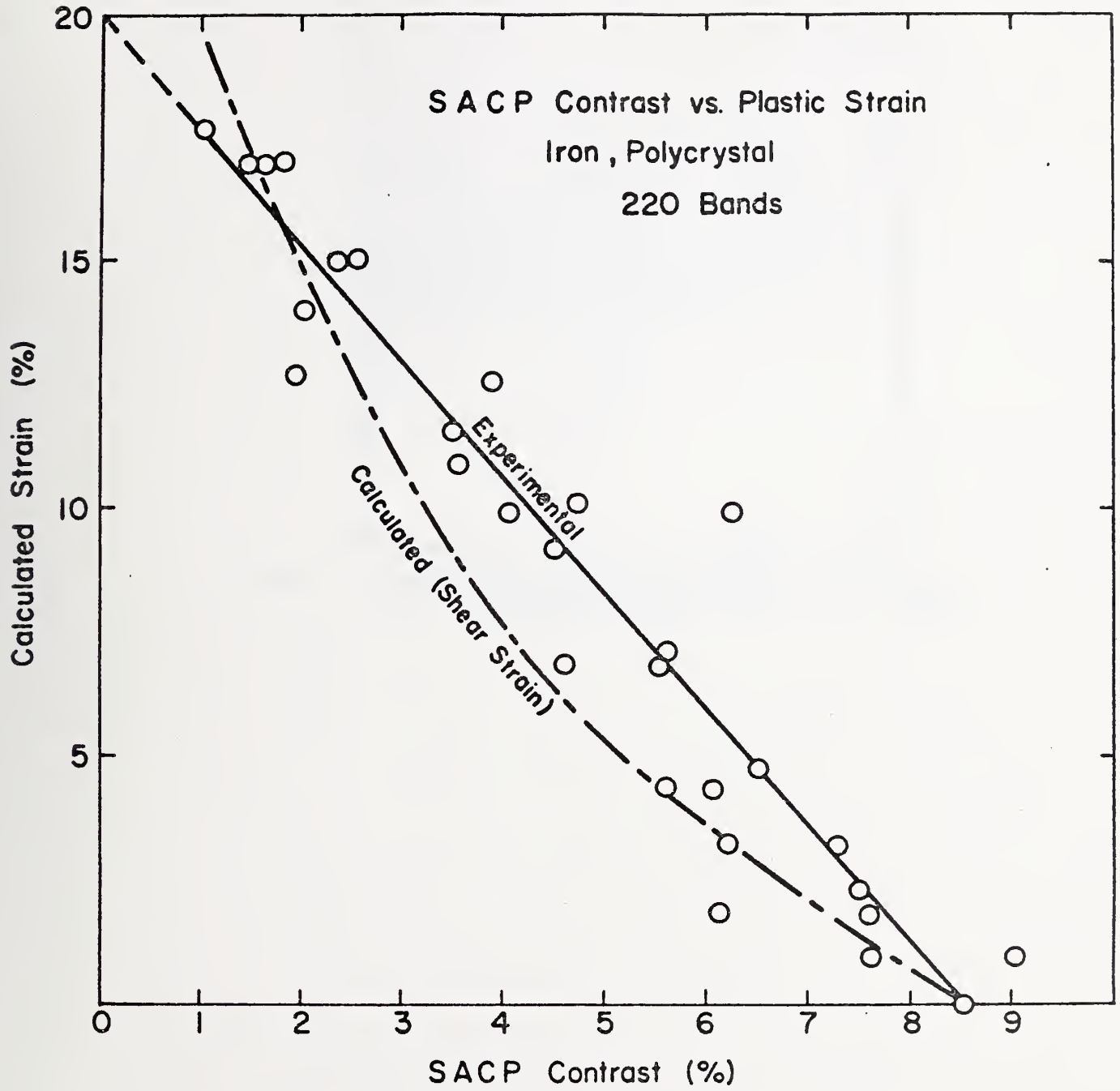

Fig. 6 Strain vs. SACP contrast determined from calibration specimen and calculated after Schulson.[13]

Fig. 7 Portion of the wear track after 1.7 m sliding in oil. Locations of SACP obtained are shown.

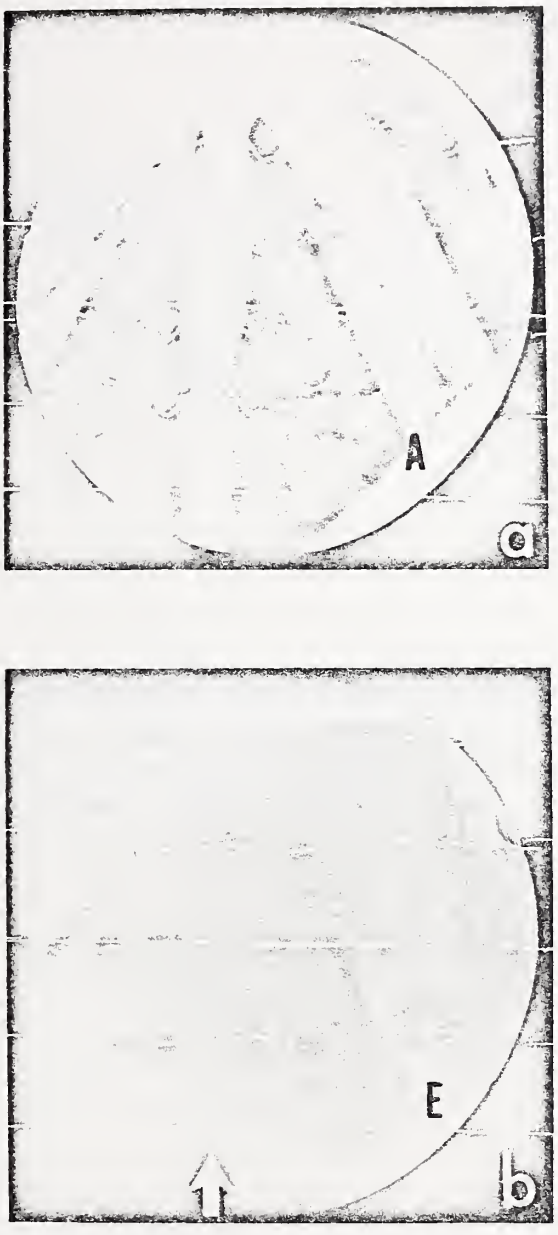

Fig. 8 SACP at locations (a) A and (b) E in previous figure. Superimposed signal traces show loss of contrast at high strain location.

Fig. 9 Portion of wear track after 17 m sliding test in oil. Note that grain boundaries are detectible beneath edge of track.

Fig. 10 Details at wear track in previous figure. Note deformation marks in pre-existing cavity in track surface.

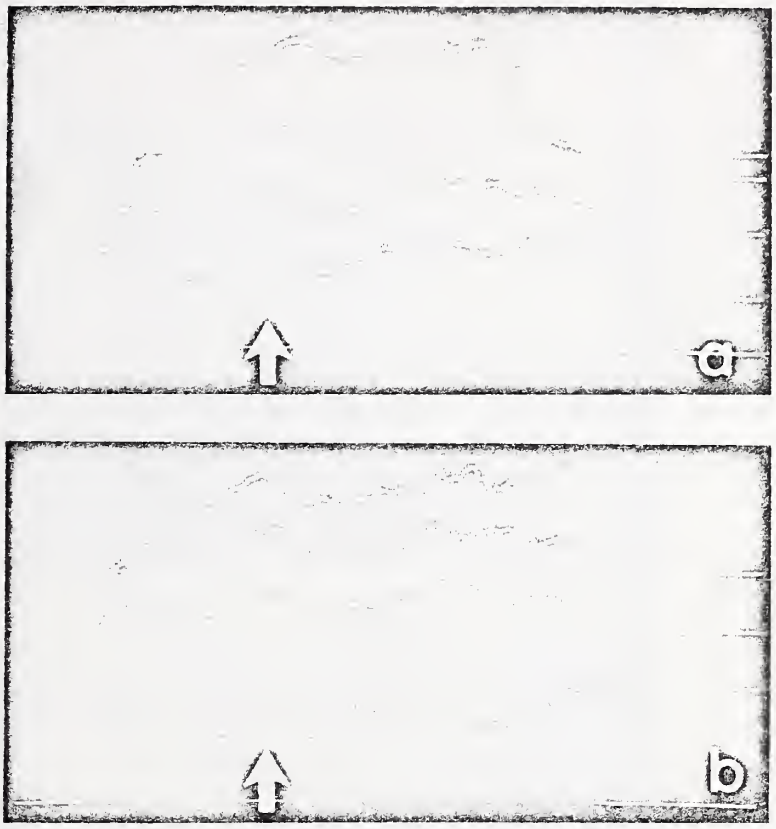

Fig. 11 SACP traces of 220 band from 17 m sliding test specimen at (a) wear track center and (b) wear track edge locations at a depth of 10 μm.

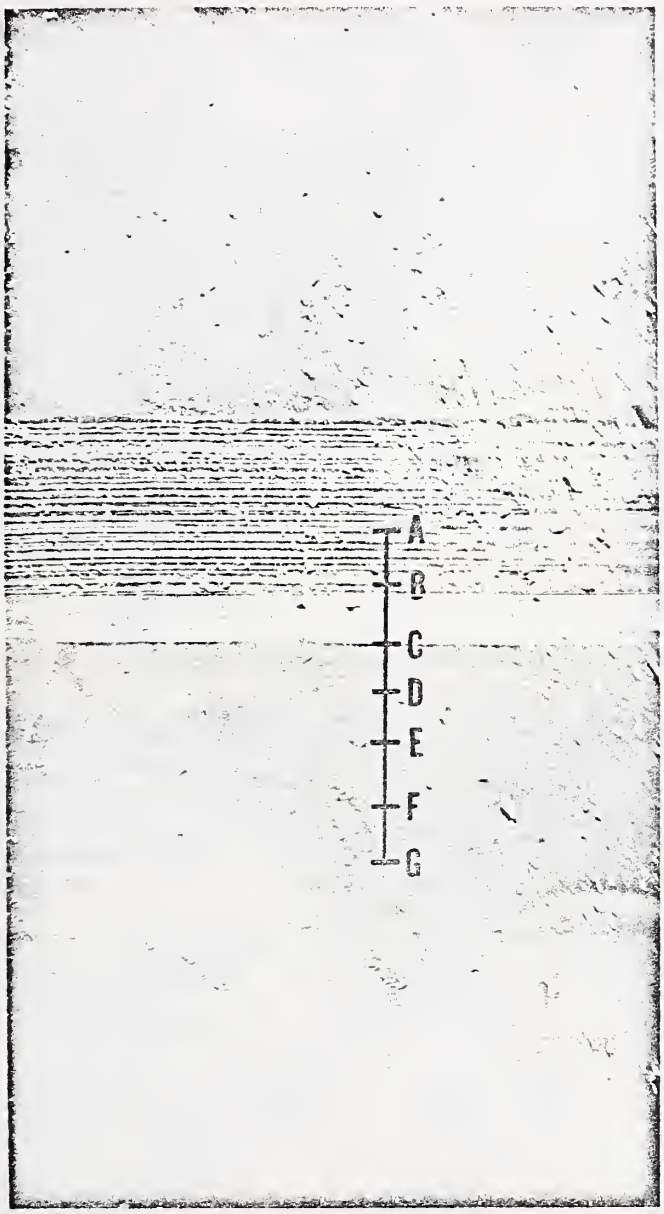

Fig. 12 Portion of wear track after 170 m sliding distance in oil. Some wear debris remains on the surface.

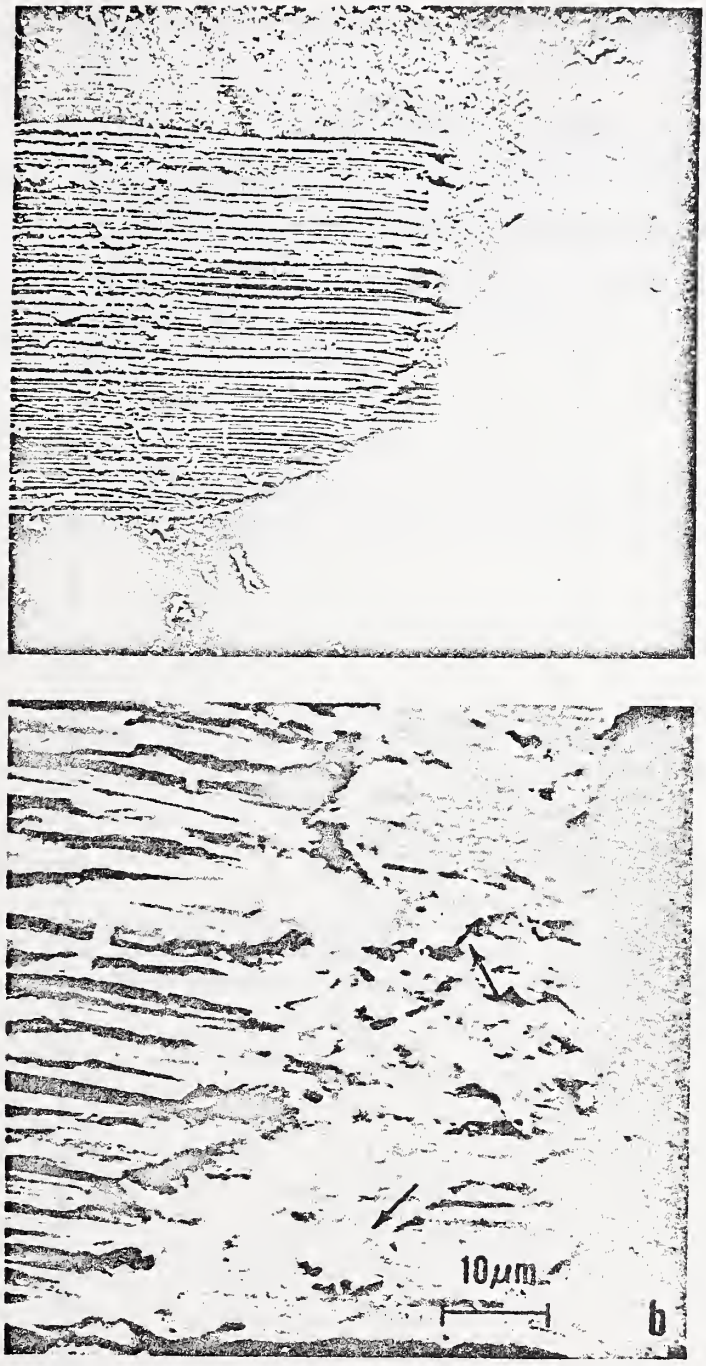

Fig. 13 Details at the wear track end in previous specimen. Two large wear debris particles are indicated. Note extensive ridge formation in wear track.

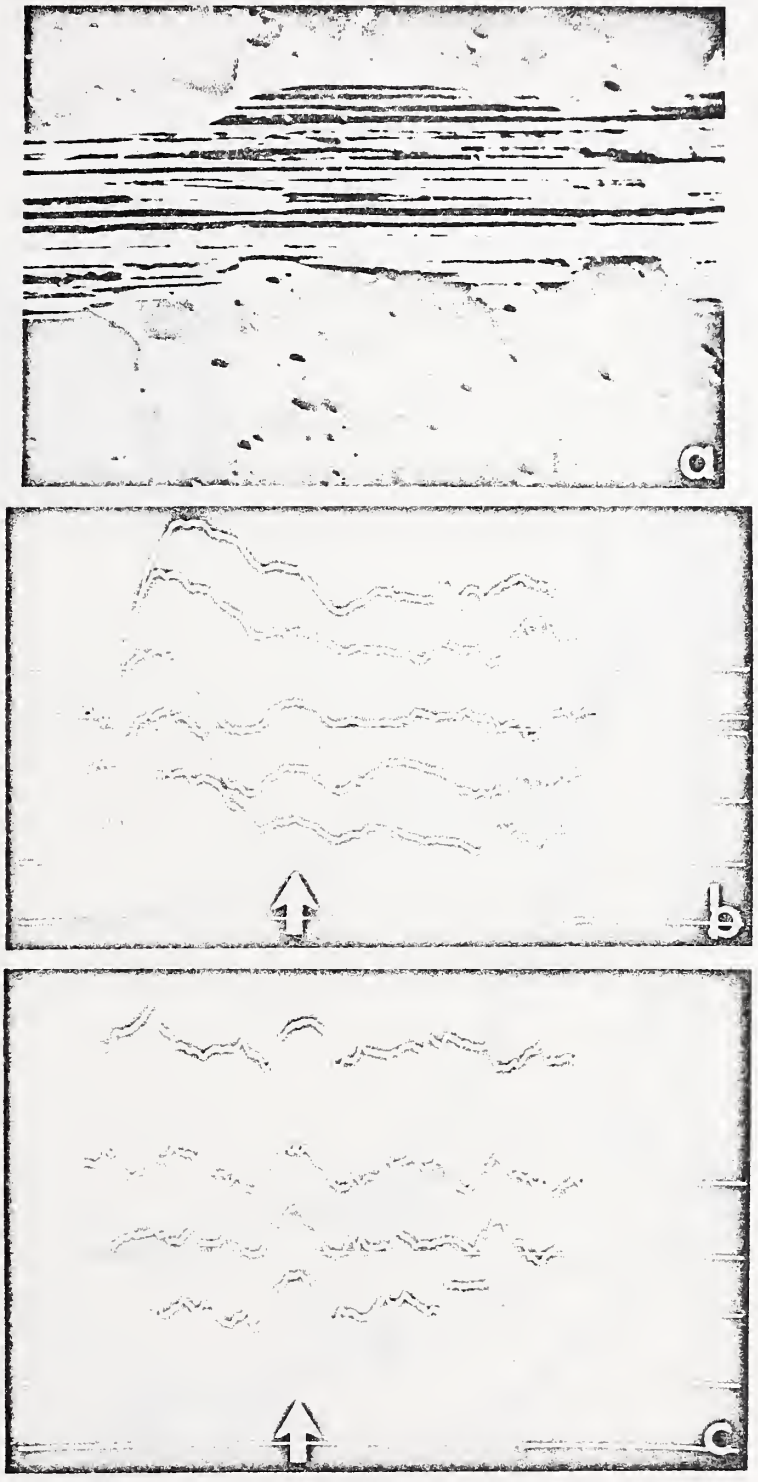

Fig. 14 (a) Wear track portion from 17 m dry sliding test. Traces from SACP obtained at (b) track edge and (c) at one track width distance.

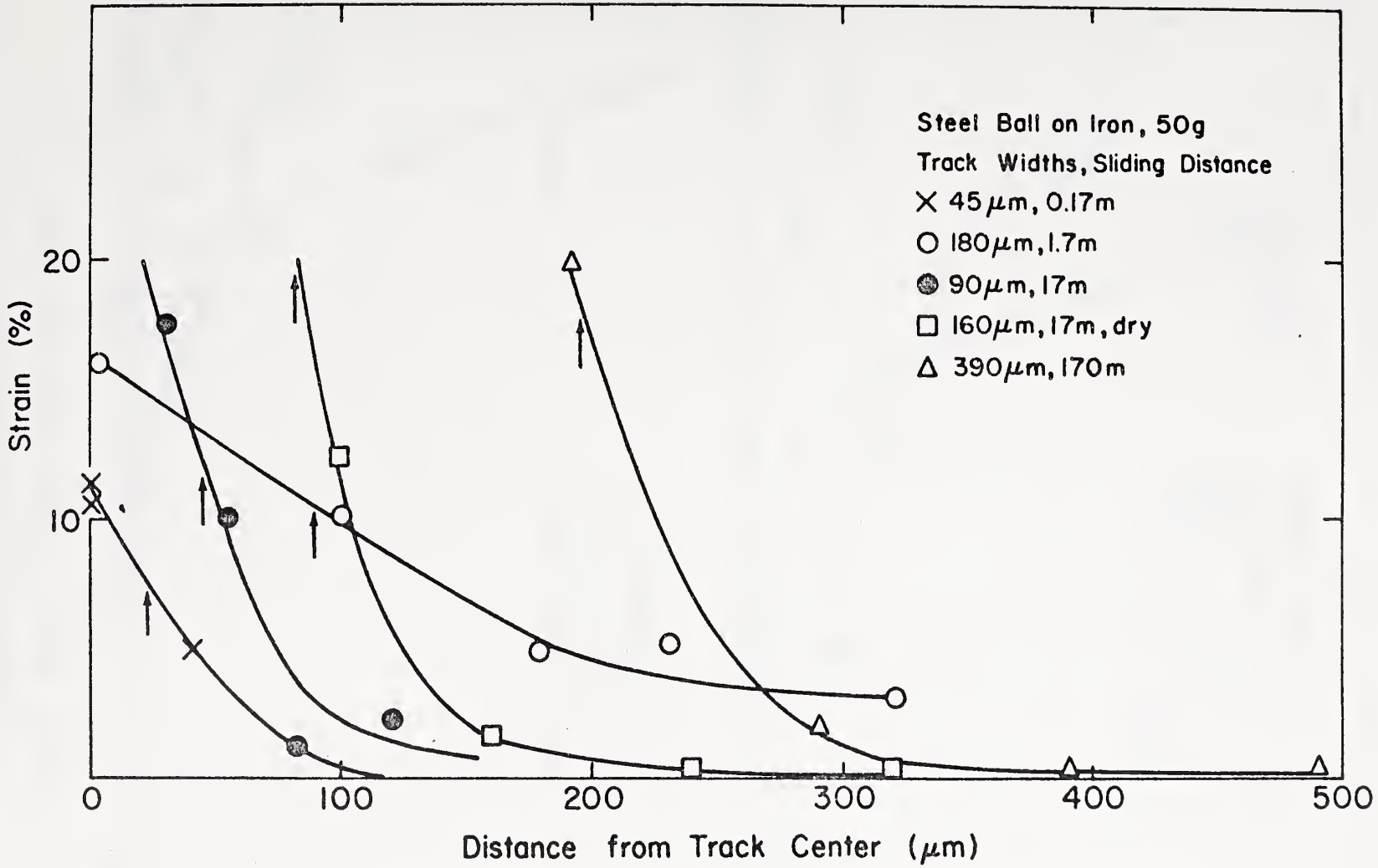

Fig. 15 Strain determinations for various sliding distances and wear track locations.

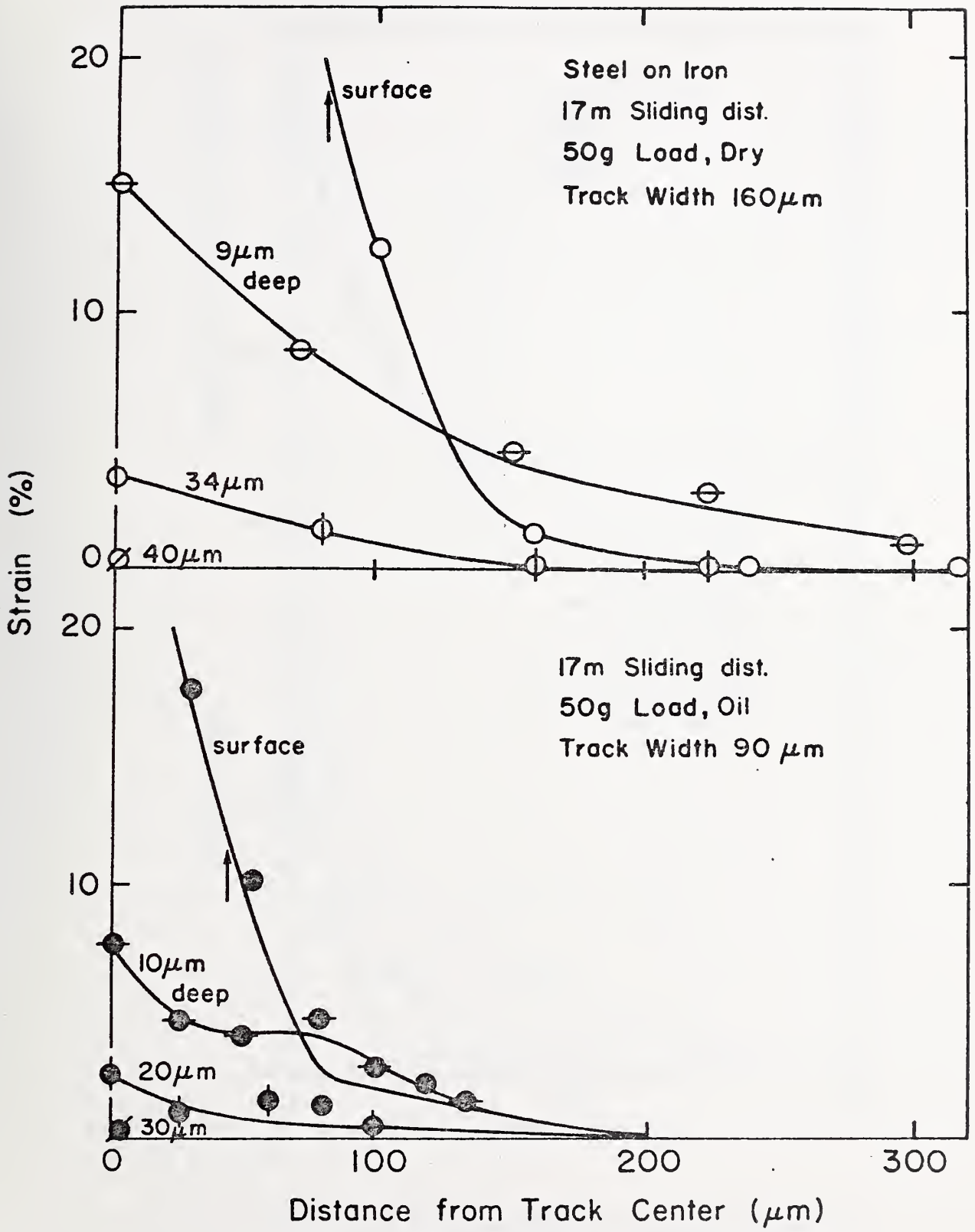

Fig. 16 Strain determinations at and beneath the original surface for dry and oil-lubricated wear tests.

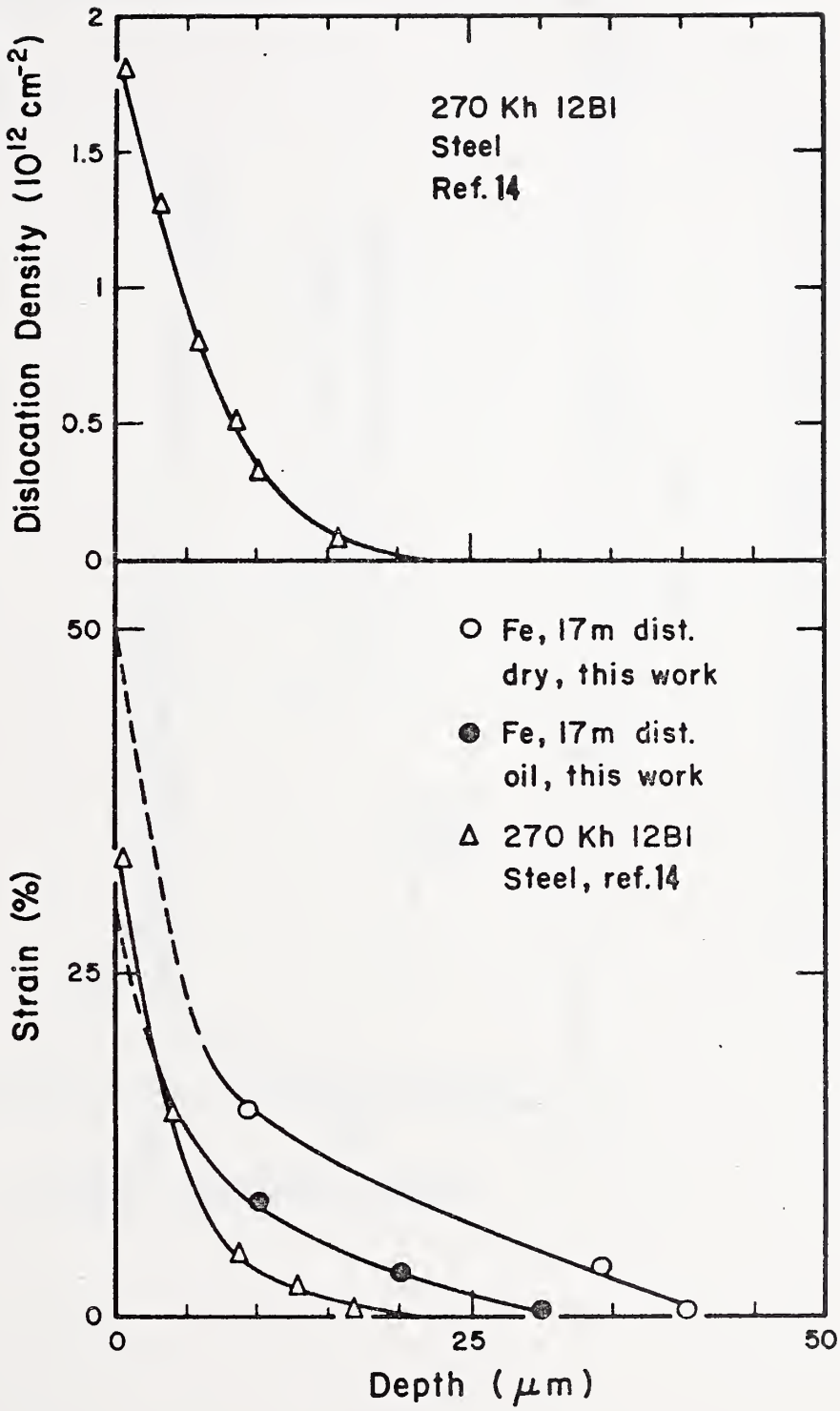

Fig. 17 Dislocation density and strain comparison between present work and Ref. 14

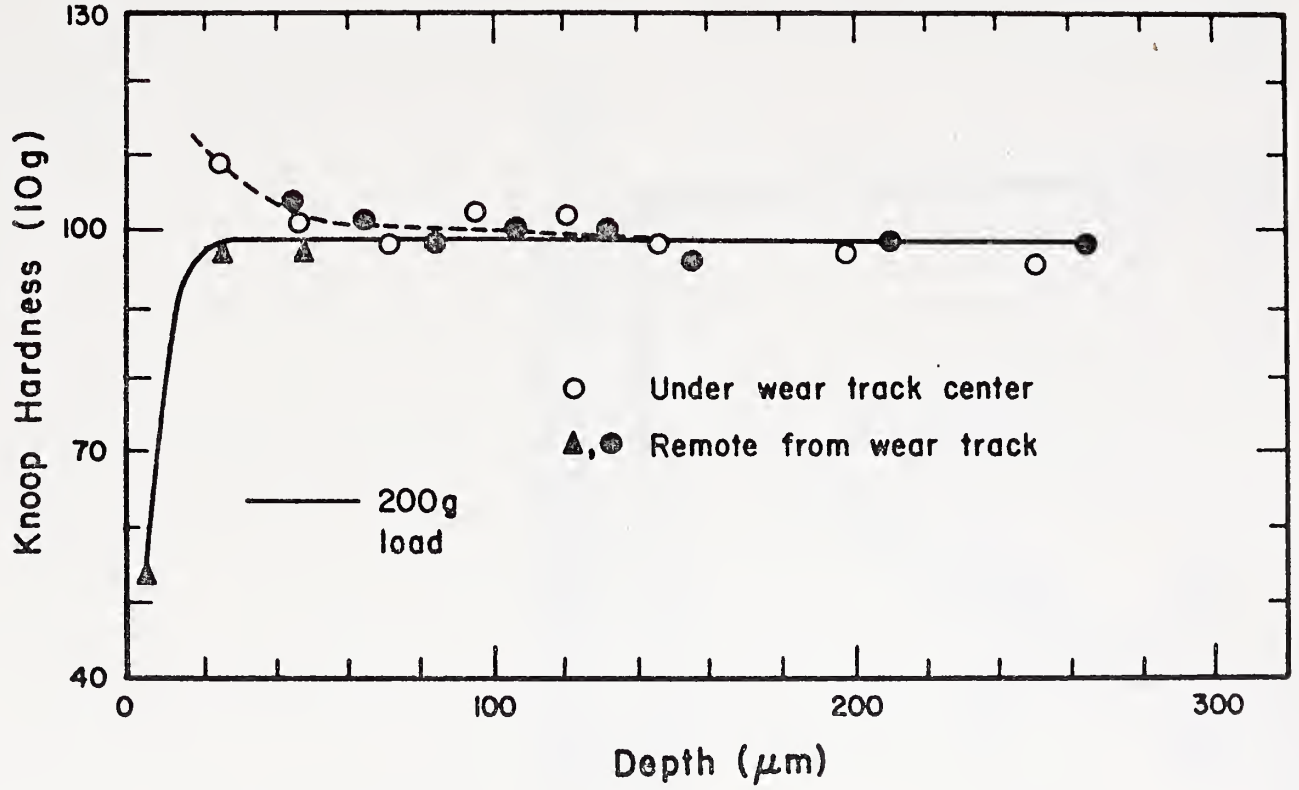

Fig. 18 Microhardness measurements on wear test specimen comparing material at and distant from wear track.

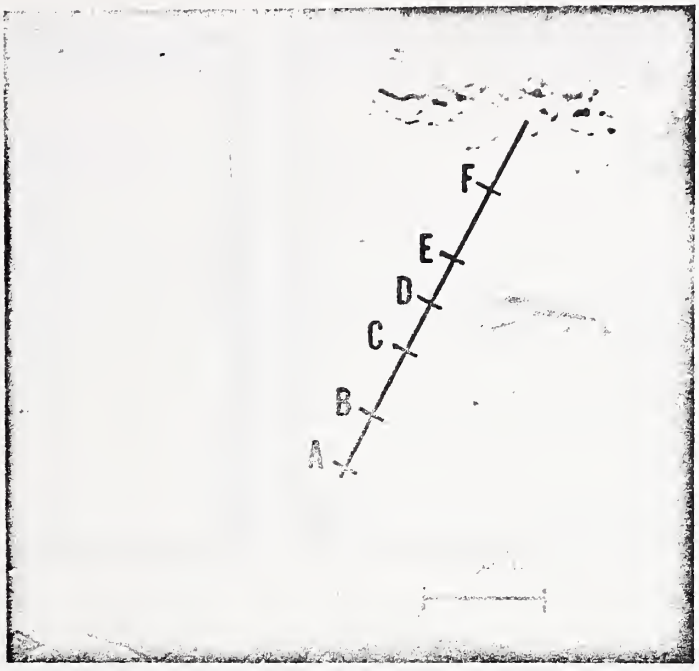

Fig. A1 Area of indentation mark on specimen surface and locations from which SACP were obtained.

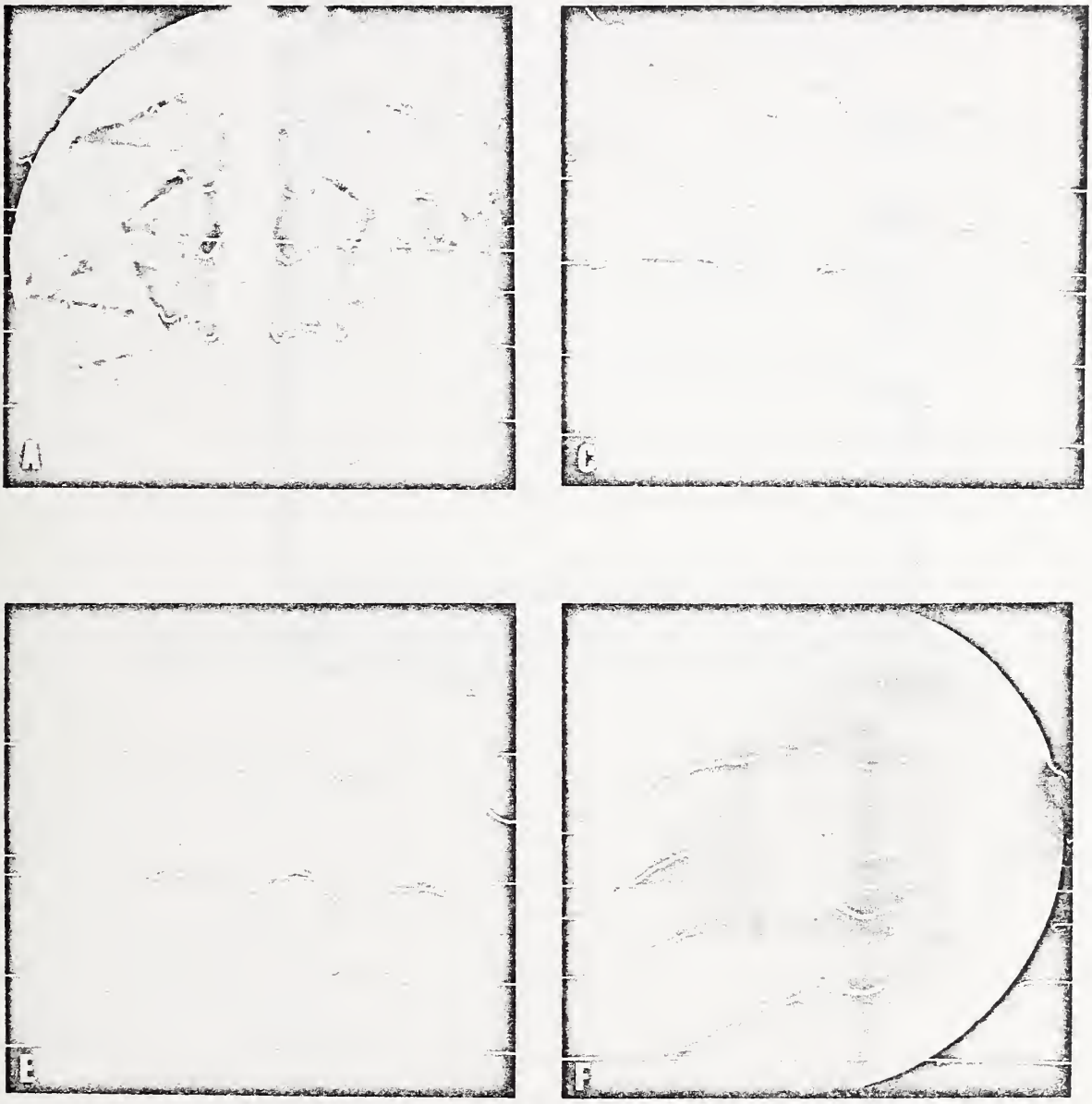

Fig. A2 Four SACP from indicated positions at a depth of 70 μm below original surface.

Fig. A3 Area of indentation mark at a depth of 120 μm below the original surface after electropolishing.

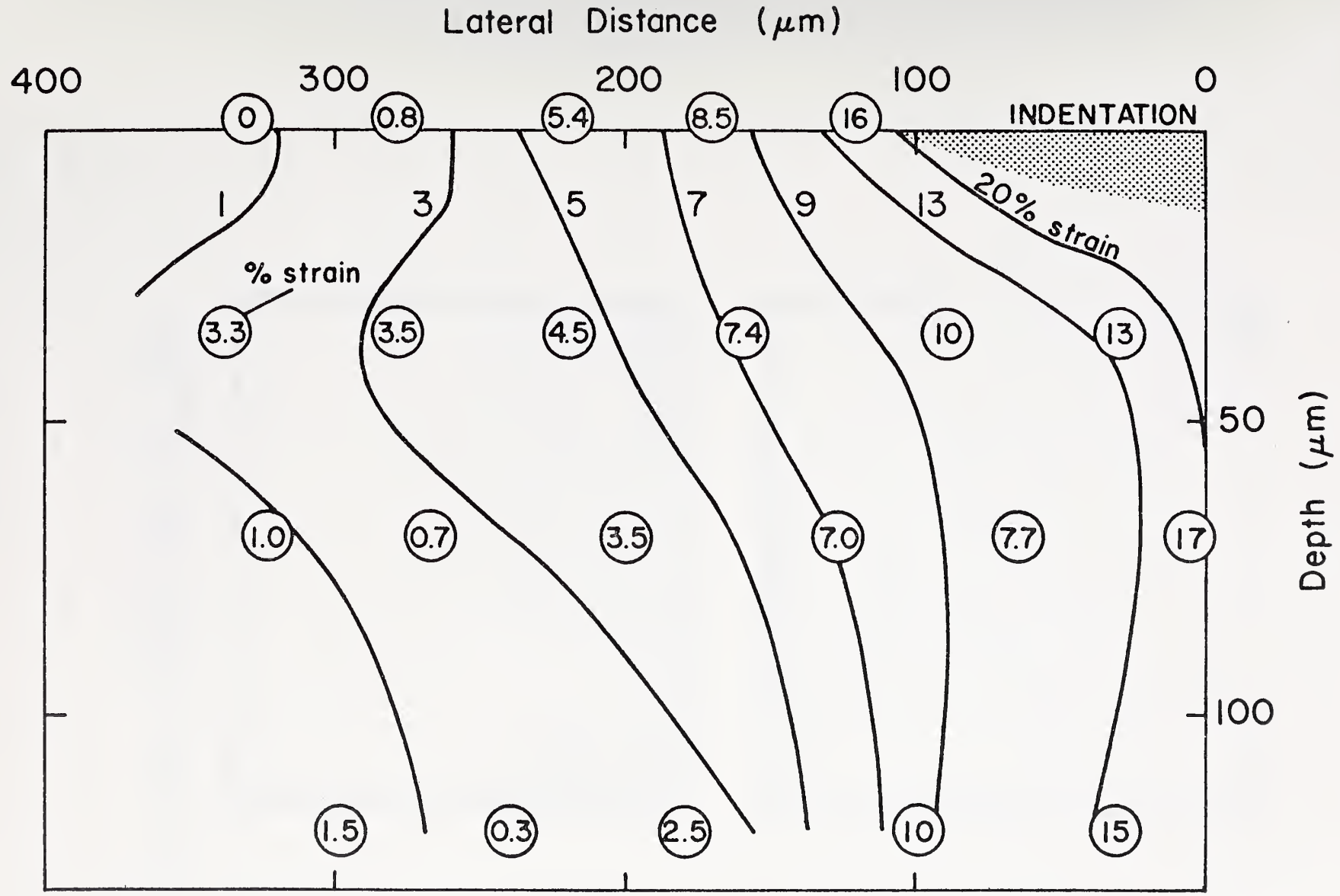

Fig. A4 Configuration of strains determined in a vertical plane through the indentation mark. Solid lines are approximate strain contours.

Fig. B1 (a) Electropolished surface of iron single crystal. (b) SACP of specimen, angular range 5 deg., near (113) orientation.

DISTRIBUTION LIST

	NO. OF COPIES
Office of Naval Research Arlington, Virginia 22217 Attn: Code 411, R. S. Miller	1
Office of Naval Research Contract Administrator, Southeastern Area 2110 G Street, N.W. Washington, D. C. 20037	1
Director Naval Research Laboratory Washington, D. C. 20375 Attn: Technical Information Division Code 2029	6 6
Defense Documentation Center Building 5 Cameron Station Alexandria, Virginia 22314	12
Air Force Materials Lab Wright-Patterson Air Force Base Dayton, Ohio 45433 Attn: Mr. F. Brooks	1
Department of Mechanical Engineering University of Virginia Charlottesville, Virginia 22091 Attn: P. Allaire	1
Department of Mechanical Engineering Chico State College Chico, California Attn: C. W. Allen	1
NASA-Lewis Research Center 21000 Brookpark Road Cleveland, Ohio Attn: W. J. Anderson	1
U. S. Steel Corporation Applied Research Lab Mailing Station 63 Monroeville, Pa. 15146 Attn: C. A. Bailey	1
Esso Research and Engineering Co. P.O. Box 51 Linden, New Jersey 07036 Attn: A. Beerbower	1

Mechanical Engineering Department
Massachusetts Institute of Technology
Cambridge, Mass. 02139
Attn: B. G. Bightmire 1

E. E. Bisson
20785 Eastwood Avenue
Fairview Park, Ohio 44126 1

Sibley School of Mechanical Engineering
Cornell University
Ithaca, New York 14850
Attn: J. E. Booker 1

Westinghouse Research Labs
Beulah Road
Churchill Boro
Pittsburgh, Pa. 15235
Attn: P. H. Bowen 1

Department of Mechanical Engineering
Georgia Institute of Technology
Atlanta, Georgia 30332
Attn: J. M. Bradford 1

General Electric Company
Silicon Products Department
Waterford, New York
Attn: E. D. Brown, Jr. 1

Naval Research Laboratory
Washington, D. C. 20375
Attn: R. C. Bowers, Code 6050 1

NASA-Lewis Research Center
21000 Brookpark Road
Cleveland, Ohio 44135
Attn: D. A. Buckley 1

Department of Mechanical Engineering
and Astronautical Sciences
Northwestern University
Evanston, Illinois 60201
Attn: H. S. Cheng 1

Wear Sciences Inc.
32 Sutherland Drive
Scotia, New York 12302
Attn: W. Campbell 1

Xerox Corporation
701 S. Aviation
El Segundo, California 90245
Attn: S. Chai 1

Department of Mechanical Engineering
and Astronautical Sciences
Northwestern University
Evanston, Illinois 60201
Attn: R. A. Burton 1

Institute of Fluid Mechanics
Academy of the Socialist Republic Rumania
Bucharest, Rumania
Attn: V. N. Constantinescu 1

John Deere Waterloo Tractor Works
Waterloo, Iowa 50704
Attn: P. K. Das 1

Aero Material Department
Naval Air Development Center
Johnsville, Warminster, Pa. 18974
Attn: M. J. Devine 1

Office of Naval Research
Arlington, Virginia 22217
Attn: S. Doroff 1

Virginia Polytechnic Institute
Blacksburg, Virginia 24061
Attn: N. S. Eiss, Jr. 1

Department of Mechanical Engineering
Columbia University
New York, New York
Attn: H. G. Elrod 1

IBM Corporation
Systems Products Division
Endicott, New York 13760
Attn: P. A. Engel 1

Fundamental Research Section
Research and Technical Department
Texaco Research Center
Beacon, New York
Attn: R. Fein 1

Mechanical Engineering Department
Virginia Polytechnic and State Univ.
Blacksburg, Virginia 24061
Attn: M. Furey 1

Naval Air Development Center
Johnsville, Warminster, Pa. 18974
Attn: M. K. Gabel 1

Chevron Research Company
576 Standard Avenue
Richmond, California 94800
Attn: D. Godfrey 1

Department of Mechanical Engineering
University of Virginia
Charlottesville, Va. 22091
Attn: E. J. Gunter 1

Mechanical Development Department
Research Laboratories
General Motors Corporation
Warren, Michigan 48090
Attn: D. F. Hays 1

Department of Machine Design
Technical University of Denmark
DK-2800 Lyngby, Denmark
Attn: J. Jakobsen 1

Department of Mechanical Engineering
University of Virginia
Charlottesville, Va. 22091
Attn: W. Jamaison 1

NASA-Lewis Research Center
21000 Brookpark Road
Cleveland, Ohio 44135
Attn: R. L. Johnson 1

University of Virginia
Thornton Hall
Charlottesville, Va. 22091
Attn: J. J. Kauzlarich 1

Cincinnati, Inc.
P.O. Box 11111
Cincinnati, Ohio 45211
Attn: R. A. Ketterer 1

Mechanical Engineering Department
Texas A&I University
College Station, Texas
Attn: D. F. Kettlebourgh 1

Department of Chemical Engineering
Pennsylvania State University
University Park, Pa. 16802
Attn: E. E. Klaus 1

Director, Department of Aerospace
Properties Research
Southwest Research Institute
8500 Culebra Road
San Antonio, Texas 78206
Attn: P. M. Ku 1

Department of Mechanical Engineering
Cleveland State College
Cleveland, Ohio
Attn: V. H. Larson 1

Department of Mechanics
Rensselaer Polytechnic Institute
Troy, New York 12181
Attn: F. F. Ling 1

Timken Company
1835 Dueber Avenue, S.W.
Canton, Ohio 44706
Attn: W. E. Littmann 1

Department of Mechanical Engineering
University of Michigan
Ann Arbor, Michigan 48105
Attn: K. Ludema

Department of Engineering Mechanics
North Carolina State University
Raleigh, N. C. 27607
Attn: C. J. Maday 1

Ford Motor Company
Research Laboratory
Dearborn, Michigan 48120
Attn: J. Meyer 1

Mobil Research & Development Corp.
Central Research Division
Box 1025
Princeton, N.J. 08540
Attn: W. R. Murphy 1

National Science Foundation
Engineering Mechanics Division
1800 G Street
Washington, D. C.
Attn: H. S. Ojalvo 1

Shaker Research, Inc.
Latham, New York 12110
Attn: C. T. Pan 1

NASA-Lewis Research Center
21000 Brookpark Road
Cleveland, Ohio 44135
Attn: R. Parker — 1

Wear Sciences, Inc.
32 Sutherland Drive
Scotia, New York 12302
Attn: M. B. Peterson — 1

Mechanical Engineering Department
Cornell University
Ithaca, New York 15850
Attn: R. M. Phelan — 1

Mobil Research & Development Corp.
Box 1025 Princeton, New Jersey 08540
Attn: C. N. Rowe — 1

Department of Mechanical Engineering
Georgia Institute of Technology
Atlanta, Georgia 30332
Attn: D. M. Sanborn — 1

Department of Materials Engineering
University of Illinois at Chicago Circle
Box 4348
Chicago, Illinois 60680
Attn: J. A. Schey — 1

University of Wisconsin
1513 University Avenue
Madison, Wisconsin 53706
Attn: A. Seireg — 1

Mechanical Engineering Department
Carnegie-Mellon University
Pittsvurgh, Pa.
Attn: M. C. Shaw — 1

Haic Division
Pure Carbon Co., Inc.
St. Marys, Pa. 15857
Attn: J. J. Sherlock — 1

Pratt & Whitney Aircraft (MS-EB2B)
400 Main Street
East Hartford, Conn.
Attn: R. P. Sevchenko — 1

SKF Industries, Inc.
1100 First Avenue
King of Prussia, Pa. 15857
Attn: L. B. Sibley — 1

Mechanical Engineering Department
University of Tennessee
Knoxville, Tennessee 37916
Attn: K. Stair — 1

Ford Motor Company
Research Laboratory
Dearborn, Michigan 48120
Attn: L. Ting — 1

General Electric Company
Building 55-119
Schenectady, N.Y. 12305
Attn: J. H. Vohr — 1

Manager, Bearings, Lubrication
& Seals
Mechanical Technology, Inc.
968 Albany Shaker Road
Latham, New York 12110
Attn: D. F. Wilcock — 1

Department of Mechanical Engineering
Georgia Institute of Technology
Atlanta, Georgia 30332
Attn: W. O. Winer — 1

NASA-Lewis Research Center
21000 Brookpark Road
Cleveland, Ohio 44135
Attn: E. V. Zaretsky — 1

Office of Naval Research
Arlington, Virginia 22217
Attn: P. Clarkin, Code 471 — 1
K. Ellingsworth, Code 473 — 1

Naval Ship Engineering Center
Prince George's Center
Hyattsville, Maryland 20782
Attn: L. B. Hebbard, Code 6107 — 1
R. Lane, Code 6101F — 1

Naval Air Systems Command
Washington, D. C. 20360
Attn: B. Poppert, Code 340E — 1
E. Regelson, Code 4115 — 1
H. Rosenwasser, Code 424 — 1

Chief of Naval Material
Washington, D. C. 20360
Attn: CAPT W. Holton, Code 041 1
CAPT G. D. Webber, Code 09H 1
J. Ward, 04112 1

Naval Air Engineering Center
Ground Support, Equipment Division
Philadelphia, Pa. 19112
Attn: Code SE-624, P. Senholze 1

Naval Ship Research and Development Laboratory
Annapolis, Maryland 21401
Attn: Mr. N. Glassman, Code 821 1
Mr. W. Smith, Code 2832 1

Air Force Aero Propulsion Laboratory
AFAPL/SFL
Wright Patterson Air Force Base, Ohio 45433
Attn: Mr. C. Hudson 1

National Engineering Laboratory
East Kilbridge, Glasgow (G. Britain)
Attn: Mr. D. Scott 1

National Bureau of Standards
Department of Commerce
Washington, D. C. 20234
Attn: Dr. E. Passaglia 1
Dr. W. Ruff 1

Institute of Ocean Science & Engineering
Dept. of Civil & Mechanical Engineering
The Catholic University of America
Washington, D. C. 20017
Attn: Dr. A. Thiruvengadam 1

U. S. Army Mobility Equipment Command
Directorate of Research, Development and Engineering
Fort Belvoir, Virginia 22060
Attn: Mr. A. J. Rutherford 1

Office of Secretary of Defense (I&L)
The Pentagon, Room 2B322
Washington, D. C. 20350
Attn: Mr. H. Peterson 1

AFSME Oil Analysis Section
Room 4A264, The Pentagon
Washington, D. C. 20330
Attn: COL Benjamin 1

University College of Swansea
Singleton Par,
Swansea, Wales SA28PP
Attn: Prof. F. T. Barwell 1

Massachusetts Institute of Technology
Lincoln Laboratory
Cambridge, Mass. 02139
Attn: Prof. N. Cook 1
Prof. E. Rabinowicz 1
Prof. N. Suh 1

Imperial College of Science and Technology
Dept. of Mechanical Engineering
Exhibition Road
London, England SW7
Attn: Prof. Alistair Cameron 1

AB-SVENSKA KULLAGERFABRIKEN
Group Headquarters
S-41550
Gothenberg, Sweden
Attn: Dr. A. Palmgren 1

Mr. Robert Q. Barr 1
Associate Director
Technical information
Climax Molybdenum Company
1270 Avenue of Americas
New York, N.Y. 10020

Commander
Naval Ships Systems Command
Code 045N
Washington, D. C. 20362 1

Naval Ordnance Systems Command
Code 0442
Washington, D. C. 20360
Attn: G. Tsuchida 1

Naval Ordnance Systems Command
Code ORD-04531
Washington, D. C. 20360
Attn: A. R. Romano 1

Naval Ordnance Systems Command
Washington, D. C. 20360
Attn: CDR F. Jonasz 1

Naval Ordnance Station
Code 50331
Louisville, Kentucky 40214
Attn: J. W. Patton 1

Quality Evaluation and Engineering Laboratory
NAD/Oahu (Code 3032)
FPO San Francisco 96612
Attn: Seiji Sakata 1

Commander
Cruiser Destroyer Force,
Atlantic Fleet
Code 414
Norfolk, Virginia 23511
Attn: FTCS Buchanan 1

Commander
Cruiser Destroyer Force,
Pacific Fleet
Code 434
San Diego, California 92110
Attn: Chief Collins 1

Commanding Officer
Naval Ordnance Systems Support Office, Atlantic
Building #62
Norfolk Naval Shipyard
Portsmouth, Va. 23709
Attn: J. Reidy 1

Commanding Officer
Naval Ordnance Systems Support Office, Pacific
Post Office Box 80548
San Diego, California 92138
Attn: Code 081 Clay Westfall 1

Commanding Officer
Naval Ship Engineering Center
Code 6101F
Prince George's Center
Hyattsville, Maryland 20782
Attn: E. C. Davis 1

Commanding Officer
Naval Air Rework Facility
Technical Support Center
Code 340
Naval Air Station
Pensacola, Fla. 32508
Attn: R. Purcell 1

Commander
Charleston Naval Shipyard
Metals Section,
Material Laboratory
Code 134.11
Charleston, S. C. 29408
Attn: Hillary Douglas 1

Commander
Naval Ship Repair Facility
Subic
FPO San Francisco 96612 1

Commander
Naval Ship Repair Facility
Guam
FPO San Francisco 96612 1

Department of Chemistry
University of North Carolina
Chapel Hill, NC 27514
Attn: Dr. T. Isenhower 1

Assistant Chief for Technology
Office of Naval Research, Code 200
Arlington, Virginia 22217 1

Prof. R. M. Latanision
Metallurgy Dept. 8-202
MIT
Cambridge, Mass. 02139 1

Mr. V. C. Westcott
Trans Sonics, Inc.
P. O. Box 326
Lexington, Mass. 02713 1

Dr. D. Scott
National Engineering Laboratory
East Kilbridge, Glasgow
Great Britain 1

Dr. Ranga Komanduri
Carnegie-Mellon University
Mechanical Engineering
Pittsburgh, PA 15213 1

Dr. Robert I. Jaffee
Technical Manager, Materials
Electric Power Research Institute
3412 Hillview Avenue
P. O. Box 10412
Palo Alto, CA 94304 1

Dr. Bernard H. Kear
Materials Engineering and Research Laboratory
Pratt & Whitney Aircraft
Middletown Plant
Middletown, Conn. 06457 1

Dr. F. S. Pettit
Materials Engineering & Research Laboratory
Pratt & Whitney Aircraft
Middletown Plant
Middletown, Conn. 06457 1

Dr. B. A. Wilcox
Division of Materials Research
National Science Foundation
1800 G Street
Washington, D. C. 20550 1

Dr. I. G. Wright
Metal Science Section
Battelle
Columbus Laboratories
505 King Avenue
Columbus, Ohio 43201 1

Prof. I. Finnie
Dept. of Mechanical Engineering
University of California
Berkeley, CA 94720 1

Dr. Edward Van Reuth
ARPA
1400 Wilson Blvd.
Arlington, VA 22209 1

Dr. E. Saibel
Army Research Office
P. O. Box 1221
RTP, North Carolina 27709 1

Prof. David A. Rigney
Dept. of Metallurgical Engineering
The Ohio State University
116 West 19th Avenue
Columbus, Ohio 43210 1

Security Classification

DOCUMENT CONTROL DATA - R & D

(Security classification of title, body of abstract and indexing annotation must be entered when the overall report is classified)

1. ORIGINATING ACTIVITY (Corporate author)

Dr. A. W. Ruff, Metallurgy Division
National Bureau of Standards
Washington, D. C. 20234

2a. REPORT SECURITY CLASSIFICATION

Unclassified

2b. GROUP

3. REPORT TITLE

STUDIES OF DEFORMATION AT SLIDING WEAR TRACKS IN IRON

4. DESCRIPTIVE NOTES (Type of report and inclusive dates)

Final Report (6/75 to 12/75)

5. AUTHOR(S) (First name, middle initial, last name)

A. W. Ruff

6. REPORT DATE

February 1976

7a. TOTAL NO. OF PAGES

67

7b. NO. OF REFS

24

8a. CONTRACT OR GRANT NO.

NAonr-35-75

b. PROJECT NO.

NBS 3120438

c.

d.

9a. ORIGINATOR'S REPORT NUMBER(S)

NBSIR 76-992

9b. OTHER REPORT NO(S) (Any other numbers that may be assigned this report)

10. DISTRIBUTION STATEMENT

Distribution of this document is unlimited.

11. SUPPLEMENTARY NOTES

12. SPONSORING MILITARY ACTIVITY

Department of the Navy
Office of Naval Research
Arlington, VA 22217
Attn: Lt. R. Miller

13. ABSTRACT

Determinations of strains have been made on the surface and subsurface on specimens of high purity iron after different amounts of sliding wear have taken place. The method involved the measurement of loss of intensity (contrast) of particular electron channeling lines obtained from small selected areas near the wear track. Through the use of a calibration specimen deformed plastically to a range of strain values, the channeling line contrast loss was related to plastic strain. Strain maps lateral to the wear track and below the original surface were obtained for different total sliding distances by removing controlled thicknesses of iron using electropolishing. In all cases the maximum strain was found at the track center location at the surface and the strains decreased steadily with depth below the track. At 50 g load the strains vanished at about 40 μm depth. Significant strains were found to exist outside the wear track boundaries. The results are compared with other studies previously reported. There was no indication of a soft or less hardened surface layer in any of the specimens studied.

NBS-114A (REV. 7-73)

U.S. DEPT. OF COMM. BIBLIOGRAPHIC DATA SHEET	1. PUBLICATION OR REPORT NO. NBSIR 76-992	2. Gov't Accession No.	3. Recipient's Accession No.

4. TITLE AND SUBTITLE

Studies of Deformation at Sliding Wear Tracks in Iron

5. Publication Date February 1976

6. Performing Organization Code

7. AUTHOR(S) A. W. Ruff

8. Performing Organ. Report No.

9. PERFORMING ORGANIZATION NAME AND ADDRESS

NATIONAL BUREAU OF STANDARDS
DEPARTMENT OF COMMERCE
WASHINGTON, D.C. 20234

10. Project/Task/Work Unit No. 3120438

11. Contract/Grant No. NAonr-35-75

12. Sponsoring Organization Name and Complete Address (Street, City, State, ZIP)

Department of the Navy
Office of Naval Research
Arlington, VA 22217

13. Type of Report & Period Covered Final Report 1/75 to 12/75

14. Sponsoring Agency Code

15. SUPPLEMENTARY NOTES

16. ABSTRACT *(A 200-word or less factual summary of most significant information. If document includes a significant bibliography or literature survey, mention it here.)*

Determinations of strains have been made on the surface and subsurface on specimens of high purity iron after different amounts of sliding wear have taken place. The method involved the measurement of loss of intensity (contrast) of particular electron channeling lines obtained from small selected areas near the wear track. Through the use of a calibration specimen deformed plastically to a range of strain values, the channeling line contrast loss was related to plastic strain. Strain maps lateral to the wear track and below the original surface were obtained for different total sliding distances by removing controlled thicknesses of iron using electropolishing. In all cases the maximum strain was found at the track center location at the surface and the strains decreased steadily with depth below the track. At 50 g load the strains vanished at about 40 μm depth. Significant strains were found to exist outside the wear track boundaries. The results are compared with other studies previously reported. There was no indication of a soft or less hardened surface layer in any of the specimens studied.

17. KEY WORDS *(six to twelve entries; alphabetical order; capitalize only the first letter of the first key word unless a proper name; separated by semicolons)*

Electron channeling; iron; metals; plastic deformation; surfaces; wear.

18. AVAILABILITY

[X] Unlimited

[ ] For Official Distribution. Do Not Release to NTIS

[ ] Order From Sup. of Doc., U.S. Government Printing Office Washington, D.C. 20402, SD Cat. No. C13

[X] Order From National Technical Information Service (NTIS) Springfield, Virginia 22151

19. SECURITY CLASS (THIS REPORT) UNCLASSIFIED

21. NO. OF PAGES 69

20. SECURITY CLASS (THIS PAGE) UNCLASSIFIED

22. Price $4.50